Construction and Building Materials 407 (2023) 133533

Contents lists available at ScienceDirect

Construction and Building Materials

journal homepage: www.elsevier.com/locate/conbuildmat

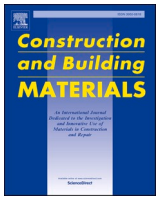

Acorn gasification char valorisation in the manufacture of alkali activated materials

M.A. Gómez-Casero [a,b,*], Luís Calado [c,d], Pedro Romano [c,d], D. Eliche-Quesada [a,b]

[a] Department of Chemical, Environmental and Materials Engineering, Higher Polytechnic School of Jaén, University of Jaén, Campus Las Lagunillas s/n, 23071 Jaén, Spain
[b] Center for Advanced Studies in Earth Sciences, Energy and Environment (CEACTEMA), University of Jaén, Campus Las Lagunillas s/n, 23071 Jaén, Spain
[c] IPPortalegre – Polytechnic Institute of Portalegre, Campus Politécnico 10, 7300-555 Portalegre, Portugal
[d] VALORIZA – Research Centre for Endogenous Resource Valorization, Polytechnic Institute of Portalegre, 7300-555 Portalegre, Portugal

ARTICLE INFO

Keywords:
Alkali activated cements
Acorn gasification char
Electric arc furnace slag
Circular economy

ABSTRACT

The use of biomass for energy production is becoming increasingly common. An energy source with good prospects for the future is the gasification process of biomass waste. This process is characterized by the partial oxidation of the raw material at high temperatures, which converts the raw material into a mixture of combustible gases. However, one of the problems when using biomass is the ash produced in the gasification process. This study investigates the effect of the incorporation of ash generated in the production of syngas from biomass residues from the acorn industry on the physical, mechanical and thermal performance of electric arc furnace slag (EAFS) based alkaline activated cements for industrial applications. Acorn gasification ash (AGA) after a calcination process were used to replace EAFS at different substitution ratios: 0, 25, 50, 75 and 100 wt%. The influence of the modulus of the activator (Ms = SiO_2/K_2O = 0.89; 1.38 and 1.84) was also studied. The specimens were evaluated for density, porosity, flexural and compressive strength, thermal conductivity, X-ray diffraction analysis, infrared spectroscopy, and microstructure development at 1, 7, 28 and 56 days of curing. The results showed that the inclusion of up to 50 wt% AGA gives rise to cements with similar or higher compressive strength than the control cement containing only EAFS. The optimum activator modulus depends on the proportion of precursors used, increasing with increasing AGA content. Therefore, the activator ratio and AGA content are factors that must be considered simultaneously to achieve the optimum compressive strength. The main reaction product was C-(A)-S-H gel, and to a lesser extent K-(A)-S-H gel and C-K-(A)-S-H hybrid gel. This work suggests the use of AGA improve alkali activated metallurgical slag binders, partially substituting the conventional Portland cement as structural material.

1. Introduction

Numerous investigations are exploring innovative methods of obtaining energy cleaner and more environmentally friendly sources of energy. One of these strategies involves the utilization of biomass for the production of fuels, electricity, and H_2 gas, which has been recognized as a valuable approach for generating energy from biomass [1]. There exist various processes for converting biomass into fuel, such as biomechanical conversion and thermochemical conversion. Among these, thermochemical conversion is considered the most advantageous as it obviates the need for complex pre-treatment [2]. Thermochemical conversion encompasses processes such as torrefaction, pyrolysis and gasification. The gasification involves the production of synthetic gas from solid biomass and can be carried out in oxygen-deficient or low-oxygen environments, thereby reducing dioxin emissions [1]. This process is characterized by the partial oxidation of the raw material at high temperatures, typically ranging from 600 to 1000 °C, resulting in the conversion of material into a mixture of combustible gases [3]. In addition to coal, other feedstock such as biomass, petroleum or petroleum coke can also be employed to produce carbon monoxide and hydrogen [4].

The Spanish cork oak forest represents an open forest dehesa (agrosylvopastoral) involvedly shaped and sustained through human intervention and livestock activities. Spanning approximately 3.2

* Corresponding author at: Department of Chemical, Environmental and Materials Engineering, Higher Polytechnic School of Jaén, University of Jaén, Campus Las Lagunillas s/n, 23071 Jaén, Spain.
E-mail address: magomez@ujaen.es (M.A. Gómez-Casero).

https://doi.org/10.1016/j.conbuildmat.2023.133533
Received 25 April 2023; Received in revised form 7 September 2023; Accepted 24 September 2023
Available online 30 September 2023

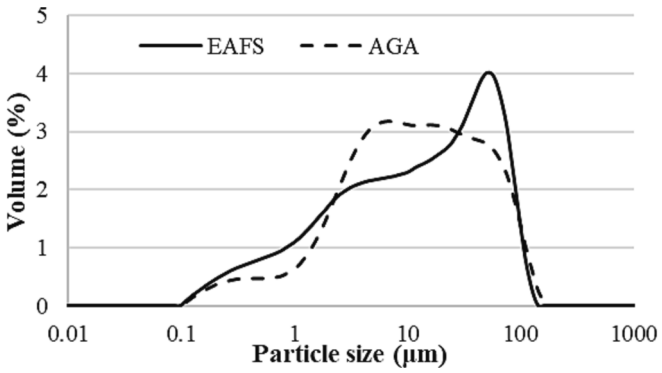

Fig. 1. Particle size distribution of raw materials.

million hectares, primarily dominated by Quercus ilex L. or Quercus suber L. trees at a density of 20–50 trees per hectare, this distinctive ecosystem is a vital component of the landscape. Particularly, approximately 40% of this expanse finds its home in the Andalusia region in Southern Spain, with the province of Huelva alone encompassing 240,585 ha of this unique environment. While the term "dehesa" is specific to Spain, analogous forests can be found in various corners of the globe, including Portugal, North Africa, and California [5].

The significance of this fruit in the Iberian economy is of such magnitude that it has prompted a proliferation of scholarly investigations within the literature. These studies aim to gain a deeper understanding of the species, the surrounding biodiversity, and the imperative for its preservation, as evidenced by the following references: [6–9]. This fruit holds paramount significance within the Iberian food industry value chain, not only due to its ability to produce gluten-free flour for breadmaking [10] and yield oil with antioxidant properties owing to its high polyphenol content [11], but also for its role in the production of premium products in the Iberian pork sector. Iberian ham, a veritable delicacy often served in thin slices to fully savour its texture and flavour, stands as an emblem of Spanish cuisine and enjoys global acclaim [12]. Furthermore, other studies delve into the acorn's medicinal applications, such as its potential in oral health [13] and its use in diabetes management [14]. This entire value chain generates substantial quantities of by-products that can be valorised through biological or thermochemical processes, such as thermal gasification.

The conversion of biomass via gasification into a combustible gas enable the utilization of this product in boilers, engines, fuel cells and as a raw material in the production of synthetic fuels or chemicals [15]. The gasification process generates two types of residues: chars and tars, which are often stored and landfilled [16]. However, novel applications have been developed for these waste products, including their use as value-added components in soil amendments, carbon sequestration, among others. [3].

On the other hand, waste from gasification process contains a significant amount of unburned carbon and oxides such as SiO_2 and/or Al_2O_3, depending of biomass source [17]. Due to the presence of aluminosilicates, they are of interest for the synthesis of alkali activated cement (AAC) or geopolymers. These materials are formed from aluminosilicates precursors through alkali silicate activation [18,19]. AAC is considered a material that could potentially replace conventional Portland cement. Ordinary Portland Cement (OPC) productions results in significant greenhouse gas emissions and consumes a substantial amount of energy [20,21]. Furthermore, OPC relies on raw materials of natural origin [22]. In contrast, AAC is of great interest because it can use materials of natural origin, industrial by-product, and other waste materials [23]. To form this compound, a precursor and an activator are necessary [24].

As materials of natural origin have been used clays [25–27], kaolin (metakaolin after calcination process) [28–30] and natural zeolites [31]. In the case of waste have been employed different metallurgical slags: steel slags [32], depending on the process, ground blast furnace slag (GBFS) can be obtained, a slag from the melting of iron into pig iron [33]; or electric arc furnace slag (EAFS) produced after melting of scrap in electric arc furnaces [34]; and other slags as carbonized high titanium slag (CHTS) [35] or copper slag (CS) [36] among others. Other wastes used to produce AAC were ash from coal combustion [30,37,38] biomass ash from forestry or agricultural industry [34,39–41], sludge [42,43], red mud [44–46], as well as other residues [47–49]. As for the activator, the most used are solutions with alkali elements in the form of hydroxide, silicate, carbonate, sulphate or a combination [50,51]. With these commercial solutions a high pH is obtained [50], which is necessary for the alkaline activation or geopolimerization process to take place, breaking covalent bonds of the source material [52].

In recent years, new research has been appearing about the use of waste from coal gasification. For instance, Xiao et al. [4] used coal gasification fly ash (CGFA) to stabilize road aggregate bases. They compared three aggregates stabilizers: ordinary Portland cement, hydrated lime and alkali activated CGFA. Yang et al. [53] used coal gasification slag (CGS) as a backfill cementitious material in coal mine backfilling, obtaining early high strength, although over time, samples suffered expansion and therefore the structure was weakened. Besides, sodium silicate has been obtained by a mechano-chemical process from coal gasification slag due to the high content of amorphous silica [16]. By other hand, CGS has been used as cementitious material to synthetize cement clinker, as supplementary material to replace cement, to manufacture bricks, thus other uses in the manufacture of construction materials [54]. Other authors developed binders incorporating CGFA into steel slag alkali activated samples [55,56]. High compressive strength due to the amorphous content in this ash were obtained. Chen et al. studied the viability of coal gasification fly ash based geopolymers to immobilize effectively heavy metals [57]. These studies demonstrate the feasibility of manufacturing of alkali activated materials by using ashes from coal gasification. This raw material can be used as a precursor in the synthesis of alkali activated materials or geopolymers and as an addition in the production of cement due to the amount of aluminosilicates present in coal gasification ashes [4]. As can be seen, most studies use coal gasification ash. However, the waste used in this study is ash from gasification process of acorn biomass. This ash have high quantity of unburned carbon, making this raw material less reactive [4] as well as, a content of aluminosilicates suitable for the synthesis of AACs.

In this study, the use of different incorporations of acorn gasification char (AGA) (0–100 wt%) as precursor in alkaline activation cements based on electric arc furnace slag (EAFS) has been investigated. The influence of the activator module Ms ratio (SiO_2/K_2O), modifying the percentages of KOH (8 M) and potassium silicate has also been studied to optimize the technological properties of binders. The results of this study demonstrate the feasibility of using gasification residues for the formation of alkali activated materials with great mechanical, physical and thermal properties has been demonstrated.

2. Materials and methods

2.1. Raw materials

The raw materials used in this study consist of two industrial by-product originating from distinct sources. The first was electric arc furnace slag (EAFS), which is a by-product of the refining process in an electric arc furnace. It was provided by Siderúrgica Balboa S.A., a company located in Jerez de los Caballeros (Badajoz, Spain). The second material was acorn gasification ash (AGA), derived from a gas extraction process involving biomass, known as gasification, and was produced at VALORIZA: Research Centre of Endogenous Resource Valorization, sited in Portalegre (Portugal).

EAFS were initially delivered with a maximum size of 4 mm, although they were crushed before in a jaw crusher. Conversely, while

Table 1
Chemical composition of raw materials.

	SiO_2	Al_2O_3	Fe_2O_3	MgO	CaO	Na_2O	K_2O	SO_3	P_2O_5	Cl	LOI
EAFS	18.59	9.44	28.61	4.56	29.45	0.2	0.04	0.4	0.38	0.21	1.39
AGA	12.36	2.95	15.61	3.02	17.1	0.57	20.17	2.49	5.01	1.17	15.84

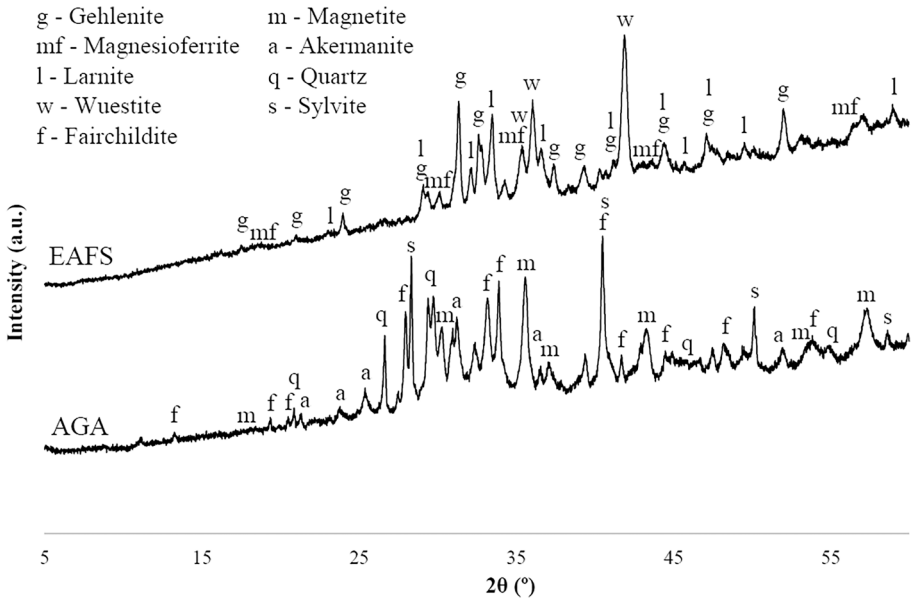

Fig. 2. Diffractograms of raw materials.

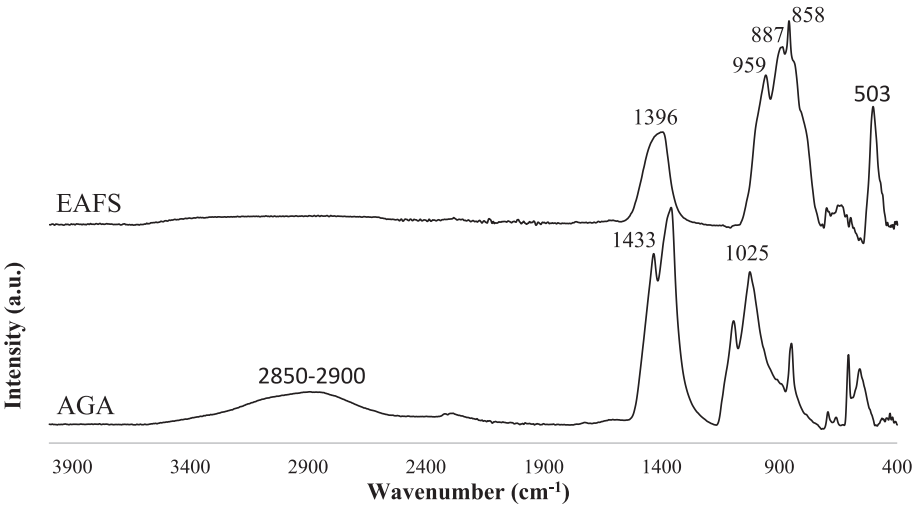

Fig. 3. FTIR spectra of raw materials.

AGA had a maximum size of 40 mm. Therefore, both materials underwent grinding in a ball mill and were sieved to achieve a particle size below 100 μm. Additionally, AGA underwent calcination at 500 °C for 4 h to remove the organic matter present in the ash.

The particle size distribution of EAFS and AGA was determined using laser diffraction analysis conducted with a Malvern Mastersizer 2000 laser diffractometer (Fig. 1). Both EAFS and AGA displayed a near-uniform distribution, with uniformity values of 1.55 and 1.62, respectively. However, there was a difference in specific surface area, with EAFS measuring 2433 m^2/kg and AGA measuring 1948 m^2/kg. The mean particle size (D_{50}) was found to be similar: with EAFS at 13.1 μm, and AGA at 12.0 μm. These values are considered suitable for the synthesis of alkali activated materials [58].

The chemical composition, determined via XRF analysis using a PW-2440 Philips Magix Pro, is presented in the Table 1. In the case of EAFS, the predominant components were CaO (29.45 wt%) and Fe_2O_3 (28.61 wt%), accompanied by a significant quantity of SiO_2 (18.58 wt%) and others components present in lesser proportions, such as Al_2O_3 (9.44 wt %), MgO (4.56 wt%) and MnO (4.18 wt%). In contrast, AGA was characterized by a prominent K_2O content (20.17 wt%) along with substantial amounts of CaO (17.1 wt%), Fe2O3 (15.61 wt%) and SiO2 (12.36 wt%). Additionally, AGA contained other components in smaller quantities, including MgO (3.02 wt%), Al_2O_3 (2.95 wt%) and SO_3 (2.49 wt%). It's noteworthy that the SO3 content in AGA falls within the limit

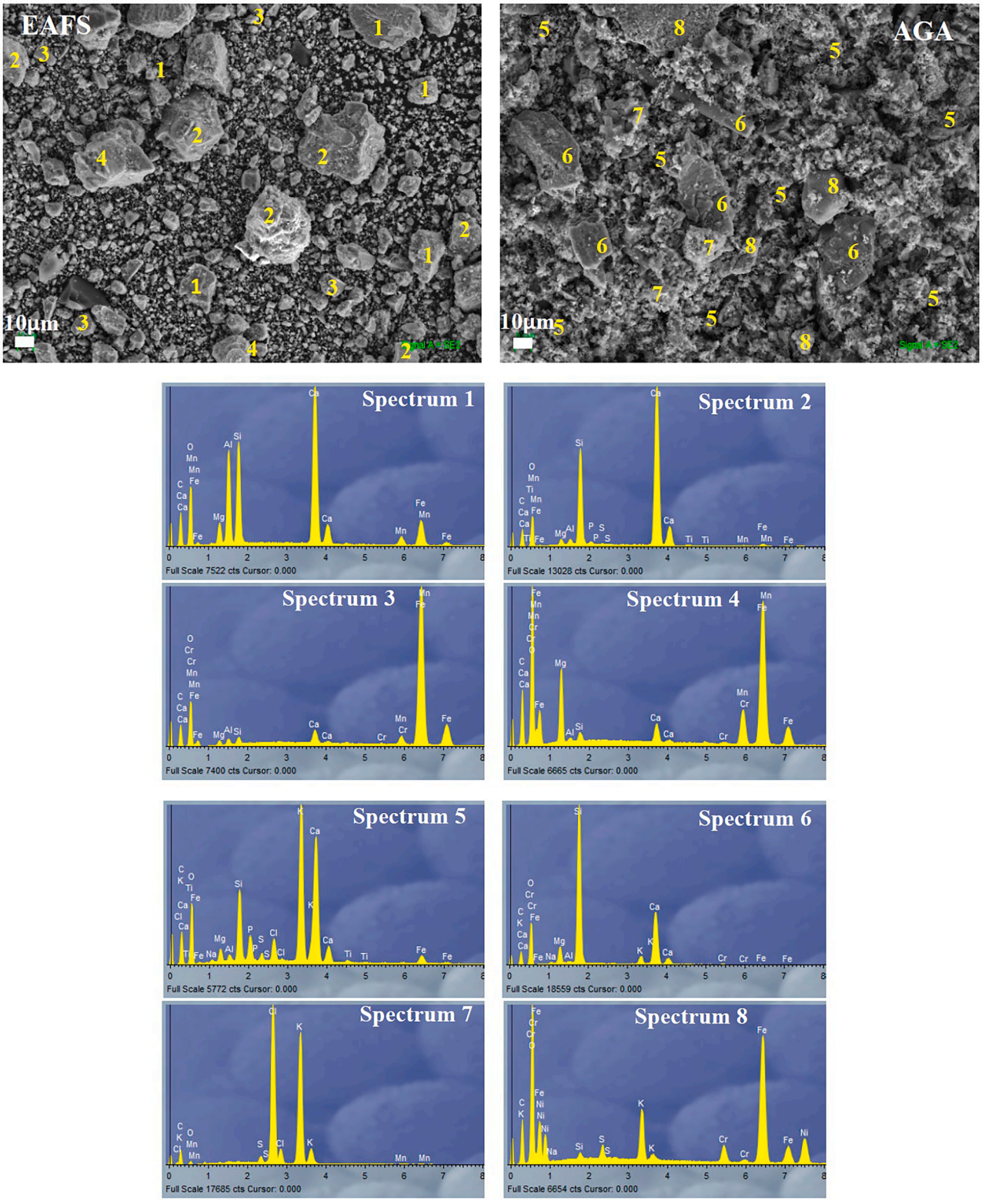

Fig. 4. SEM-EDX images of raw materials at 1000x.

established by the European standard EN 15167–1, which specifies a maximum of 2.5% for sulphates [59]. In contrast, the ASTM C618 standard sets a 5% limit for the use of supplementary cementitious materials [60]. It is worth noting that the LOI (Loss on Ignition) value of AGA was relatively high, at 15.84 wt%.

Raw materials were subjected to X-Ray Diffraction (XRD) analysis, and the results are despicted in Fig. 2. The analysis was conducted using a PANalytical Empyrean instrument equipped with a PIXcel-3D detector, and peak identification was performed using HighScore software. In addition, a semi-quantitative analysis was performed via HighScore software, without considering the amorphous phases. In the case of EAFS, the XRD analysis revealed the presence of crystalline phases such

Table 2
Dosage of activators used and Ms ratio.

Solution code	Water (g)	KOH (g)	Silicate (g)	Ms
K1	52.36	27.64	80	0.89
K2	36.65	19.35	104	1.38
K3	26.18	13.82	120	1.84

Table 3
Dosage of mixtures.

Paste code	Ash (g)	Slag (g)	Ms	Si/Al	Na_2O/SO_3
Control-K1	0	400	0.89	2.04	0.65
Control-K2			1.38	2.16	
Control-K3			1.84	2.23	
25AGA-K1	100	300	0.89	2.30	0.41
25AGA-K2			1.38	2.43	
25AGA-K3			1.84	2.52	
50AGA-K1	200	200	0.89	2.69	0.34
50AGA-K2			1.38	2.86	
50AGA-K3			1.84	2.97	
75AGA-K1	300	100	0.89	3.35	0.31
75AGA-K2			1.38	3.58	
75AGA-K3			1.84	3.74	
100AGA-K1	400	0	0.89	4.75	0.30
100AGA-K2			1.38	5.11	
100AGA-K3			1.84	5.34	

as gehlenite ($Ca_2Al(SiAl)O_7$, 25 %), larnite (Ca_2SiO_4, 37 %) and wuestite (FeO, 25 %). These crystalline phases commonly observed in this type of slag [36]. Additionally, traces of magnesioferrite ($Mg(Fe^{3+})_2O_4$, 7 %) and magnetite (Fe_3O_4, 6 %) were also detected in EAFS. As for AGA, the prominent crystalline phases identified were magnetite (27 %), fairchildite ($K_2Ca(CO_3)_2$, 41 %) and sylvite (KCl, 12 %). These findings align with previous studies using biomass ash [61,62]. In addition, lower quantities of quartz (SiO_2, 10 %) and akermanite ($Ca_2Mg[Si_2O_7]$, 10%) were identified in AGA.

Attenuated Total Reflectance Fourier Transform Infrared Spectroscopy (ATR-FTIR) was conducted on the raw materials using a Nicolet iS10 Thermo Scientific instrument. The primary bands identified in raw materials were observed centred at 1396, 858 and 503 cm^{-1} for EAFS, and at 1433 and 1025 cm^{-1} for AGA (Fig. 3). Bands centred between 1390 and 1440 cm^{-1} were assigned to the vibration modes of O—C—O bonds [63], confirming the presence of carbonates (CO_3^{-2}). The band centred at 959 cm^{-1} in the case of EAFS and 1025 cm^{-1} in AGA are attributed to the vibration mode of Si—O—T bonds (T represents tetrahedral Si or Al) [64], according to the chemical composition and glass structure. For EAFS, the most intensive peak observed at 858 cm^{-1} is associated with the stretching vibration of Ca—O and Si—O bonds [65], which is characteristic of the gehlenite [66], identified in XRD analysis (Fig. 2). Additionally, a shoulder centred at 887 cm^{-1} was identified, attributed to the asymmetric stretching of AlO_4 groups [64] The stretching bands centred between 2850 and 2900 cm^{-1} in raw materials are attributed to OH and H—O—H bonds [65].

Samples were analysed by Scanning Electron Microscope - Energy Dispersive X-Ray spectroscopy (SEM-EDX) using a JEOL SM 840 model.

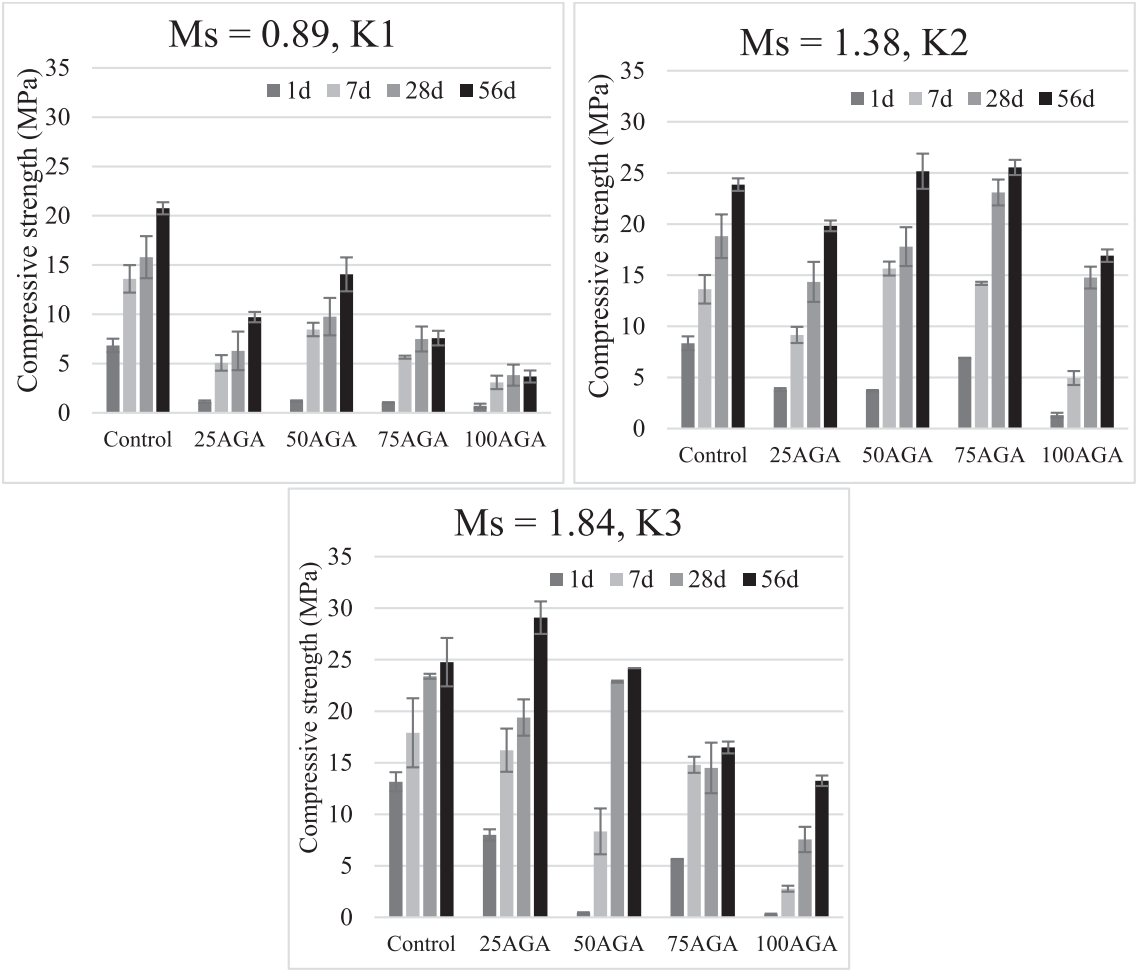

Fig. 5. Compressive strength as function of AGA content and curing time of pastes, with different Ms ratio: a) 0.89, b) 1.38 and c) 1.84.

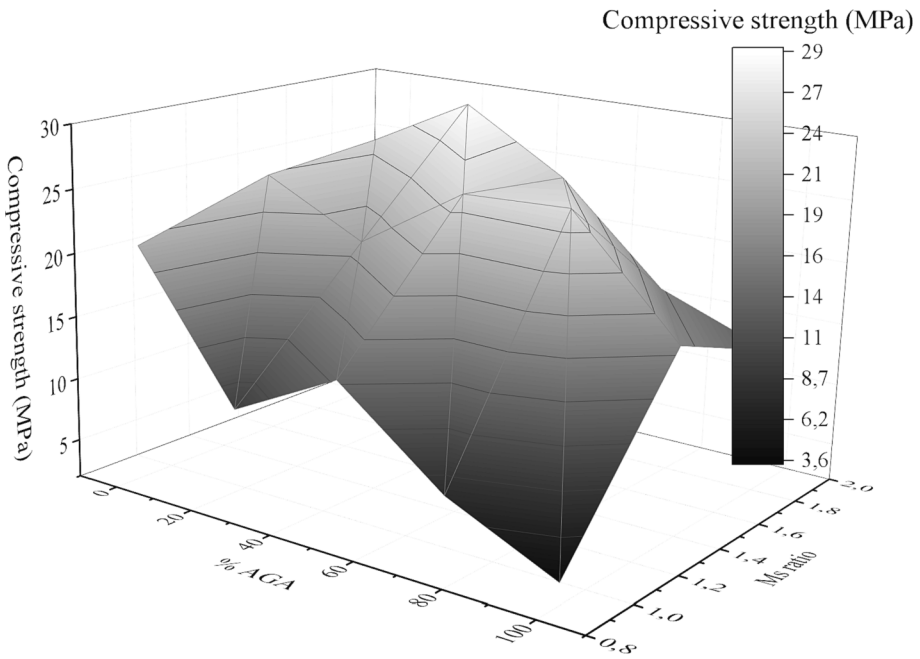

Fig. 6. 3-D plot showing the effect of Ms ratio and AGA content at 56 days of curing in compressive strength.

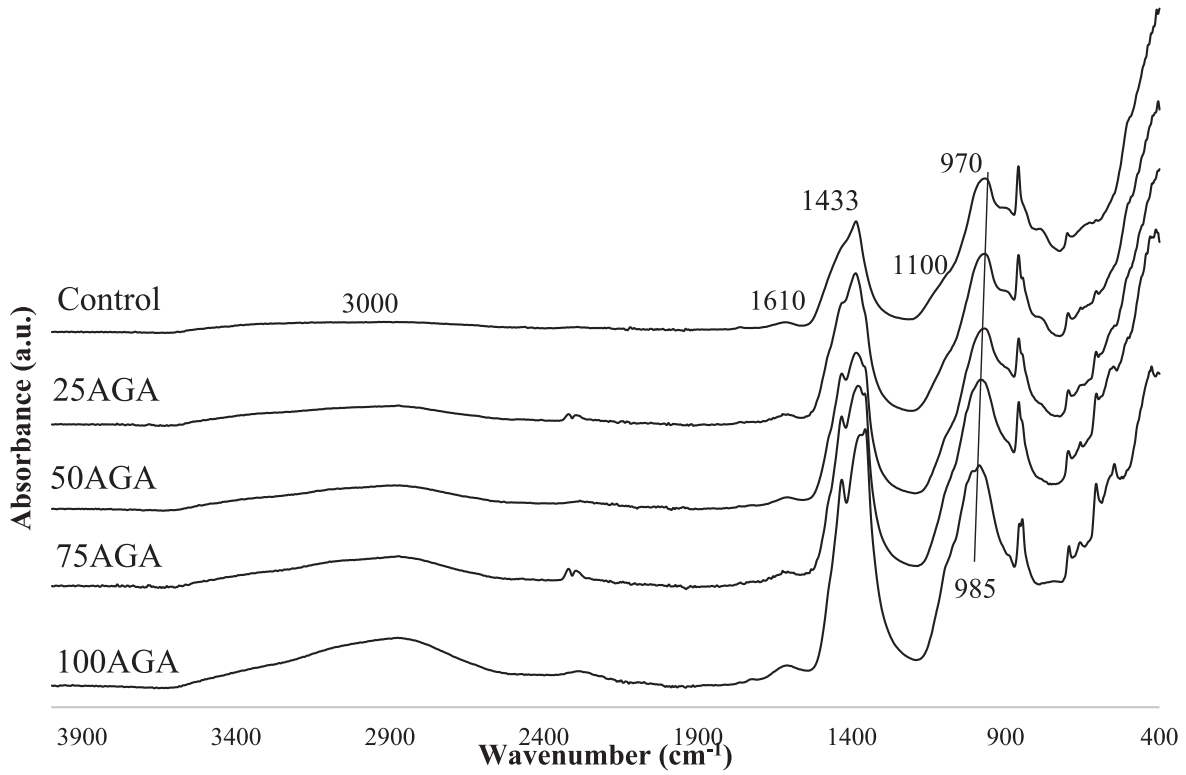

Fig. 7. FTIR spectra for samples with Ms = 1.38 at 28 days of curing as a function of AGA content.

It is evident that both raw materials exhibit similar granulometry (Fig. 4). As demonstrated in the preceding section, both materials have a relatively small mean size, which is suitable for use in the synthesis of alkali-activated materials after grinding and sieving. The materials consist of angular-shaped particles, although in the case of AGA, these are less well-defined.

In EAFS, the presence of gehlenite, larnite and iron oxides (spectrum 1, 2 and 3) was observed, primarily compounds that are found in the materials, along with traces of magnesioferrite (spectrum 4), in agreement with the XRD analysis. On the other hand, spectrums of AGA showed high quantity of Ca, Si and K, elements present in fairchildite, quartz and/or akermanite (spectrums 5 and 6). Additionally, spectrum 7 and 8 confirmed the present of KCl (sylvite) and magnetite, respectively.

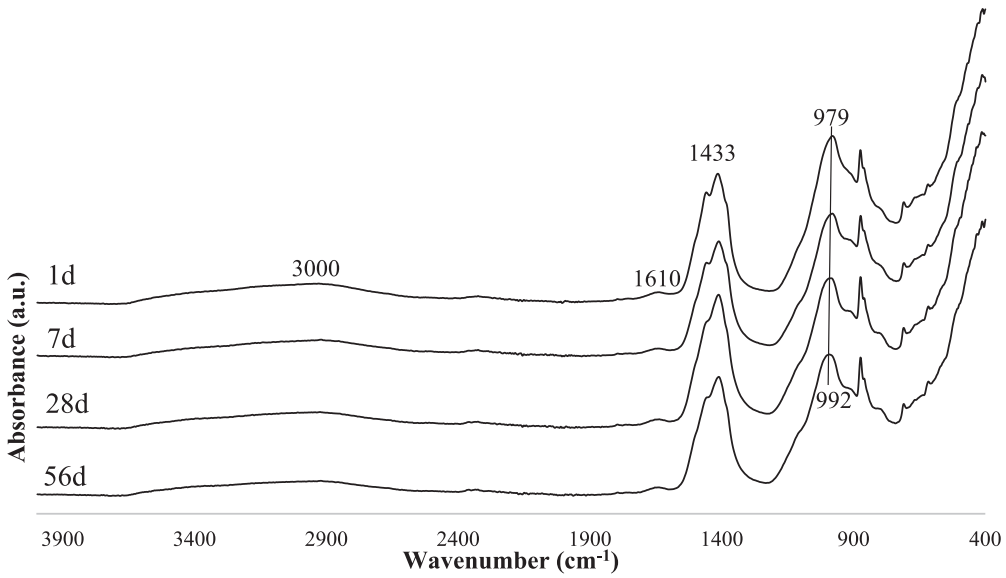

Fig. 8. FTIR spectra for 25AGA-K2 as a function of curing time.

2.2. Samples preparation

Potassium hydroxide (KOH) and potassium silicate (K2SiO3) were used as alkaline activators. Three potassium hydroxide to potassium silicate ratios were used to obtain different Ms ratio (SiO_2/K_2O). The Ms ratio is an important parameter in the manufacture of alkaline activated cements, since it affects the development of properties of the final material. Dosage of activator are shown in the Table 2. KOH pellets were delivered by GlobalChem with a purity of 85 %. Potassium silicate commercial solution was supplied by Roth company (7.5–8.7% K_2O, 19.5–21.8% SiO_2 and 69.5–73.0% H_2O). Liquid/binder ratio (l/b) was stablished in preliminary test as 0.4, and it was kept for all specimens synthetized.

The use of chars from the gasification process to enhance the properties of alkali activated cements was investigated by producing pastes with different substitutions of slag for acorn gasification ash in different proportions. In addition, control pastes consisting solely of slag were also prepared. The mixture dosage are detailed in Table 3. Each specimens was designated with the format *xAGA-Ky*, where "*x*" represented the percentage of AGA and "*Ky*" denoted the activator code. For instance, *25AGA-K2* referred to a specimen containing 25 wt% of AGA as a substitute for slag and using the K2 activator, with a Ms ratio of 1.38.

Pastes were manufactured in a planetary mixer. Precursors were mixed for duration of 90 s in order to homogeneously mix raw materials. Following this initial mixing phase, the activator solution was introduced into the mixture and further mixed for an additional 90 s. Subsequently, a scraper was employed to ensure the complete incorporation of materials adhering to the mixer walls, and an additional mixing period of 30 s was applied. The resulting materials synthetized were then transferred into moulds, which included prismatic silicone moulds measuring 15x15x10 mm and cylindrical plastic moulds with a diameter of 55 mm. Moulds with pastes were vibrated using a table shaker for 60 s to eliminate air voids. Following this, moulds were stored within the laboratory environment until the specified testing day (1, 7, 28 and 56 days of curing).

2.3. Tests developed

The prepared pastes underwent compressive strength testing in accordance with the UNE-EN 1015–11:2000/A1:2007 standard [67] using Tecnotest KD300/CE testing machine with a load capacity of 300 kN. For each specified testing day, four samples were subjected to testing. Physical properties were determined for four samples following the standard UNE-EN 1015–10 [68]. Thermal conductivity at 28 days of curing was determined for two cylindrical specimens in accordance with UNE-EN 12664:2002 [69]. This was accomplished using a FOX 50 TA instruments heat flow meter, with duplicate measurements taken.

Powdered samples were subjected to characterization using Attenuated Total Reflectance Fourier Transform Infrared Spectroscopy (ATR-FTIR) within the range of 4000 to 400 cm^{-1}. This analysis was performed using a Nicolet iS10 Thermo Scientific instrument. The identification of crystalline phases formed in the specimens were carried out through XRD analysis, and crushed surfaces of the samples after compressive strength test were further analysed using Scanning Electron Microscope (SEM) test conducted with a JEOL SM 840 model.

3. Results and discusion

3.1. Mechanical properties

Compressive strength is the most important property in structural materials. The behaviour of different proportions of replacement of EAFS by AGA were studied. Results are shown in Fig. 5 for each Ms ratio studied as a function of slag replacement and curing time. Control pastes, using only EAFS obtained maximum compressive strength of 24.8 MPa at 56 days of curing.

The highest strength was attained when employing 25 wt% of AGA as precursor. The maximum value obtained was near to 30 MPa in compressive strength at 56 days of curing. However, when 50 wt% of replacement was used, the resistance fell at 25.2 MPa at 56 days. Similar value was obtained with 75 wt% of ashes in the compound. These values are similar to those obtained by He et al. [70] at 28 days of curing. They achieved compressive strength between 27 and 35 MPa at 28 days of curing by 10 and 20 wt% CGS replacement in cement pastes. Compressive strength value decreased using 100 wt% of ashes, with the best value of 16.9 MPa at 56 days. The increase in compressive strength with the increase of slag percentage is due to C-(A)-S-H gel formation, which together with K-(A)-S-H gel form a denser matrix, thus increasing mechanical strength [71]. Focused on error bars, it can be observed that the strength deviation is smaller when the ash content is higher and using the optimal activator. In the case of control paste or 25AGA-K2 at 56 days of curing, deviations are near to 5%, while using more quantity of ashes, deviation values decrease up to 3%. Which could indicate that ashes help to stabilize the deviations of the results. This trend is also

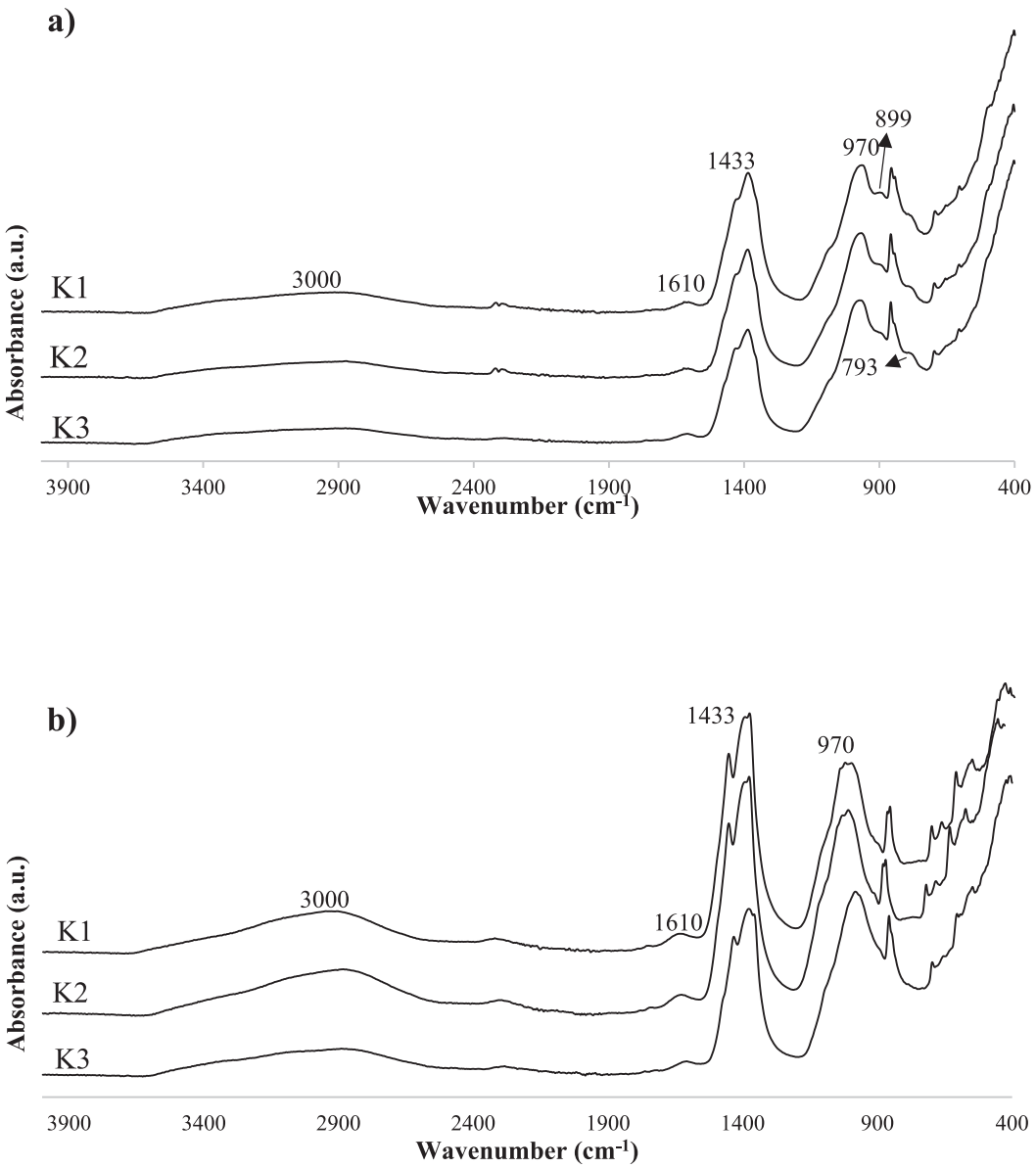

Fig. 9. FTIR spectra at 28 days of curing as a function of Ms ratio in the activator: a) 25AGA and.

observed in other works using gasification waste as raw material [70]. Using a not optimal activator deviations increase above to 10%, probably due to the instability of the gel formed.

All binders exhibited an increase in their compressive strength values as a function of curing time, owing to densification during the synthetization process [72]. The compressive strength increased with lower velocity in samples with ashes, obtaining similar results than control pastes or higher with the incorporation of 25 or 50 wt% of AGA [56]. The significant SO_3 content had an impact on the mixtures with AGA at early ages, reducing the compressive strength, although this effect was not appreciated at older ages [60,73]. In addition, SO_3 content of AGA favoured the alkali activation of slags [74]. For this reason, samples with 25 wt% of AGA achieved higher results than control pastes. A Na_2O/SO_3 ratio less than 0.5 (see Table 3) helped to obtain better properties [75]. Another parameter that affected to strength developed and gel formation were the high content of LOI and Cl [76]. LOI content produces a decrease on mechanical properties and slower hydration kinetics [77,78], while Cl had a negatively influence on matrix development [79]. Therefore, higher compressive strengths are obtained in samples containing 25 wt% of AGA, possibly due to an adequate SO_3 content and and lower LOI and Cl content. In addition, high amount of LOI and Cl drop the durability of steel and other fibres used in reinforced composites [76].

The influence of Ms ratio on compressive strength was also studied (Fig. 6). The optimal range of compressive strength values for the different compositions varied between 1.38 and 1.84 (activator K2 and K3, respectively). High activator ratio has a positive effect in the solution of calcium from waste used (EAFS and AGA) leading to the formation of a greater amount of C-(A)-S-H gel [80]. Additionally, the dissolution process of Si and Al present in raw materials contributed to the formation of geopolymeric gel K-(A)-S-H. In addition high Ms ratio provide a greater amount of extra silicate to form a gel structure, and EAFS have higher demand of potassium silicate than AGA for activation at room temperature. Optimal compressive strength values for Ms ratio of 1.84 were obtained for control samples and samples incorporating up to 50 wt% of AGA. Therefore, the Ms ratio and EAFS/AGA proportion have a synergistic influence to obtain optimum compressive strength. Low Ms ratio (Ms = 0.89, K1) can have negative effect on compressive strength, due to a weak dissolution of reacting species.

In control specimens and AACs with 25 wt% and 50 wt% of AGA, K3

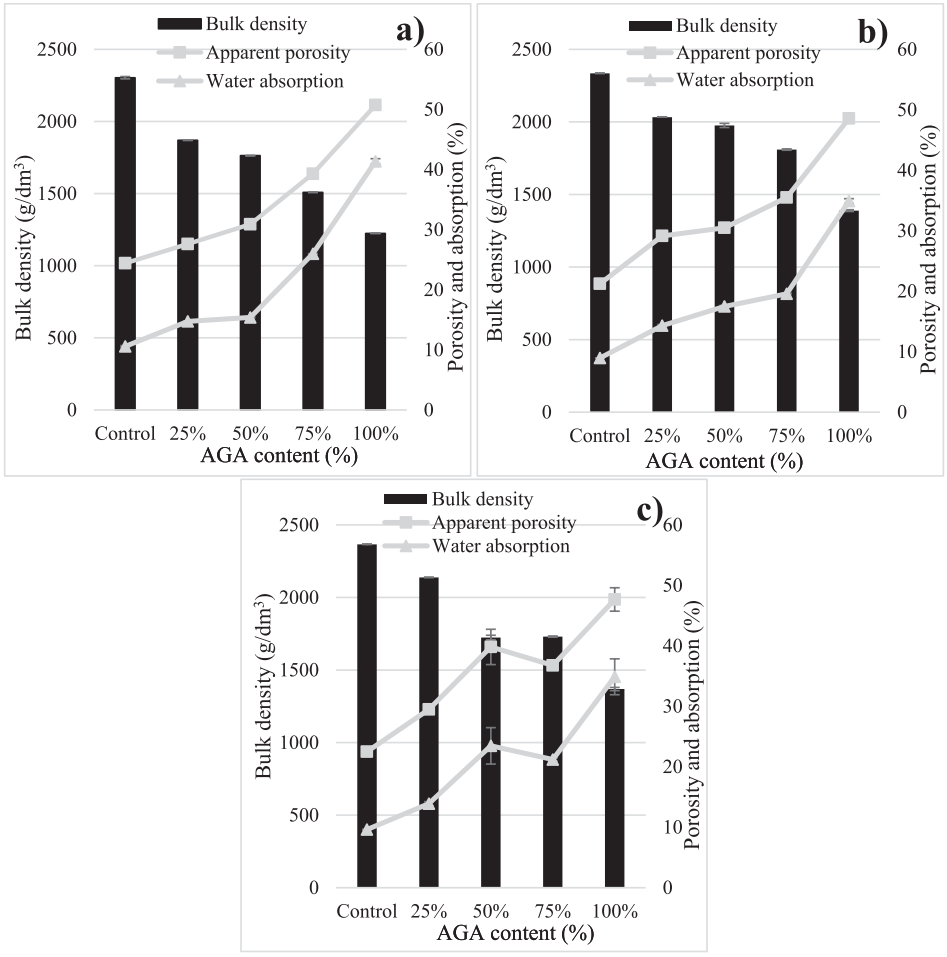

Fig. 10. Physical properties at 56 days of curing with different AGA content: a) K1, b) K2 and c) K3.

proved to be the optimal activator, yielding the best mechanical properties across all samples. Samples with 75 wt% of AGA and 100 wt% of AGA developed higher strength (25.5 and 16.9 MPa, respectively at 56 days of curing) using K2 as optimal activator. Samples with high AGA content have a high Si/Al ratio, which together with a high silicate ratio due to an increase in the Ms ratio up to 1.84, produced an increase in paste viscosity. The matrix developed was less homogenous, with more content of unreacted particles and more porous, obtaining less mechanical strength results [23]. This trend was not observed in specimens with greater EAFS content, which increased the compressive strength with the increase of Ms ratio, according to Rafeet et al. [71].

The optimum Ms values obtained for the activation of these precursors differ from those reported in other studies using Na_3SiO_2 and NaOH. Soutsos et al. [81] used a solution of sodium silicate and NaOH to activate slag blends with 13 different fly ashes, obtaining different optimum Ms values ranging from 1.00 to 1.25. In this range, Zhang et al. [82] obtained the optimal value, specifically Ms = 1.2, for mortars manufactured from metakaolin and fly ash as precursors, and NaOH and Na_3SiO_2 solution as activator, with Ms varying between 1.1 and 1.6. The same Ms value was determined in another studio using fluid catalytic cracking catalyst residue as precursor and a solution of sodium hydroxide and sodium silicate as activator, using Ms ratios between 0.7 and 2.33 [83].

3.2. Functional groups analysis: FTIR-ATR

Functional groups analysis via FTIR-ATR of pastes synthetized are shown in the Fig. 7. In this analysis, bands centred between 900 and 1200 cm^{-1} are attributed to Si—O—T bonds (T = Si or Al) stretching vibrations [84]. This band is centred at around 970 cm^{-1} in control paste. The replacement of EAFS by AGA produced a displacement of this band to higher frequencies (around 985 cm^{-1} using ash solely) [71,85] This main peak is associate to amorphous gel in alkali activated materials (M–A–S–H gels, M = Ca or K) [86,87]. Low frequencies in this band are attributed to C-(A)-S-H gel (range 950–990 cm^{-1}) [88]. At 1100 cm^{-1} appear a shoulder, which is more pronounced when more slag is used. This shoulder is attributed to alkaline gel (K-A-S-H gel) [89].

Absorption band observed in AACs, regardless of the amount of AGA added, with Ms ratio of 1.34 and 1.89, are centred at 793 cm^{-1} and are associated with symmetric stretching of Si—O—Si bonds [90], present in C-A-S-H gel. However, when Ms ratio decrease up to 0.89, this band disappear and it appear a new band around 899 cm^{-1} assigned to Si-OH bending vibrations [91], due to reduction of extra silica in the activator and the increase of alkalinity caused by decrease of Ms ratio.

The presence of OH groups were confirmed with bands centred around 3000 and 1610 cm^{-1}, related with the reaction products (hydrated phases) [65,92]. The band centred at 1610 cm^{-1} is and not present in raw materials. These bands intensify with curing time [64]. In addition, the hump centred between 2500 and 3500 cm^{-1} is more pronounced the higher ash content. Besides it was observed that the hardening times are shortened, affecting to strength developed. On the other hand, the band centred at 1433 cm^{-1} is associated with the presence of carbonates (CO_3^{-2} groups), O—C—O bonds [64,72].

Fig. 8 illustrates the FTIR spectra of 25AGA-K2 as a function of curing time. The intensity of bands centred at 3000 and 1610 cm^{-1} increased with curing time, as a consequence of alkaline activated process and the

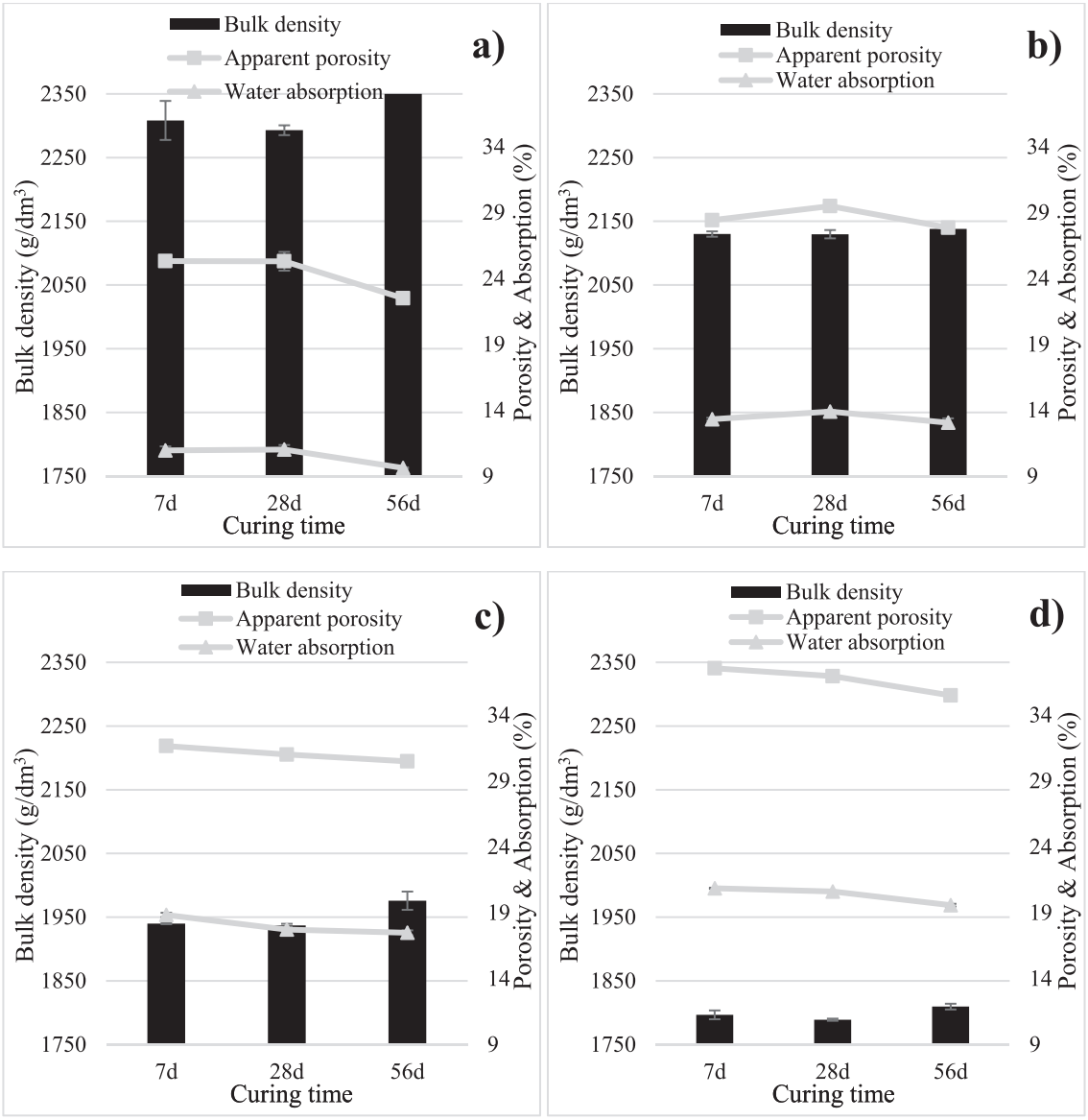

Fig. 11. Physical properties as a function of curing time: a) Control-K3, b) 25AGA-K3, c) 50AGA-K2 and d)75AGA-K2.

increase of hydration products with time. [92]. Although at 1 day of curing present a high intensity, due to fresh state of paste. The band centred at 970–990 cm^{-1} also increased with curing time, indicating the formation of C-(A)-S-H gel [93].

In Fig. 9, FTIR spectres of 25AGA and 75AGA at 28 days of curing, varying the Ms ratio employed are presented. In the specimens, elevated absorptions bands assigned to Si—O—Si bonds (970 cm^{-1}) were observed for optimal values of Ms ratio, K3 and K2, respectively, according to other authors. Hui-Teng et al. [65] used ladle furnace slag (LFS) and fly ash (FA) with different percentages and Ms ratio, and they found an optimal value for Ms = 1.5. Upper and lower Ms resulted in a lower intensity of the absorption band corresponding to Si—O—Si bonds. Furthermore, the centre of this band moves to higher wavenumber values with increasing Ms, as also found by other authors. [93,94]. This could explain the formation of a greater amount of gel when the optimal Ms is used in the activator. The hump between 2500 and 3500 cm^{-1}, it was also observed that it is more pronounced when higher Ms ratio was used in the activator.

3.3. Physical properties

Fig. 10 displays physical properties as bulk density, apparent porosity and water absorption as a function of EAFS replacement by AGA, with different Ms ratio. Bulk density decrease with AGA addition independently of Ms used, possibly due to different between real densities of raw materials: 3576 kg/m^3 and 2316 kg/m^3, for EAFS and AGA, respectively. Control-K3 paste has a bulk density of 2335 kg/m^3 at 56 days. The total replacement of slag with ash, specimens with 100 wt% of AGA produced a significant reduction of the bulk density, decreasing up to 1369 kg/m^3. Similar trend was achieved with other activator. The presence of carbonates and sulphates in ashes caused a flash setting of pastes [60] which affected the densification, decreasing their bulk density and mechanical strength, as well as producing an increase in the porosity. In addition, results suffered greater deviations when an activator with high Ms ratio and high content of ash were used. Deviations using K1 or K2 obtained errors less to 0.5% for all physical properties. While samples activated by K3 activator reached deviation up to 3% in apparent porosity and water absorption, and near to 1% in bulk density.

Bulk density increased with curing time for all specimens, due to the densification process [34], see Fig. 11. In the case of Control-K3, values

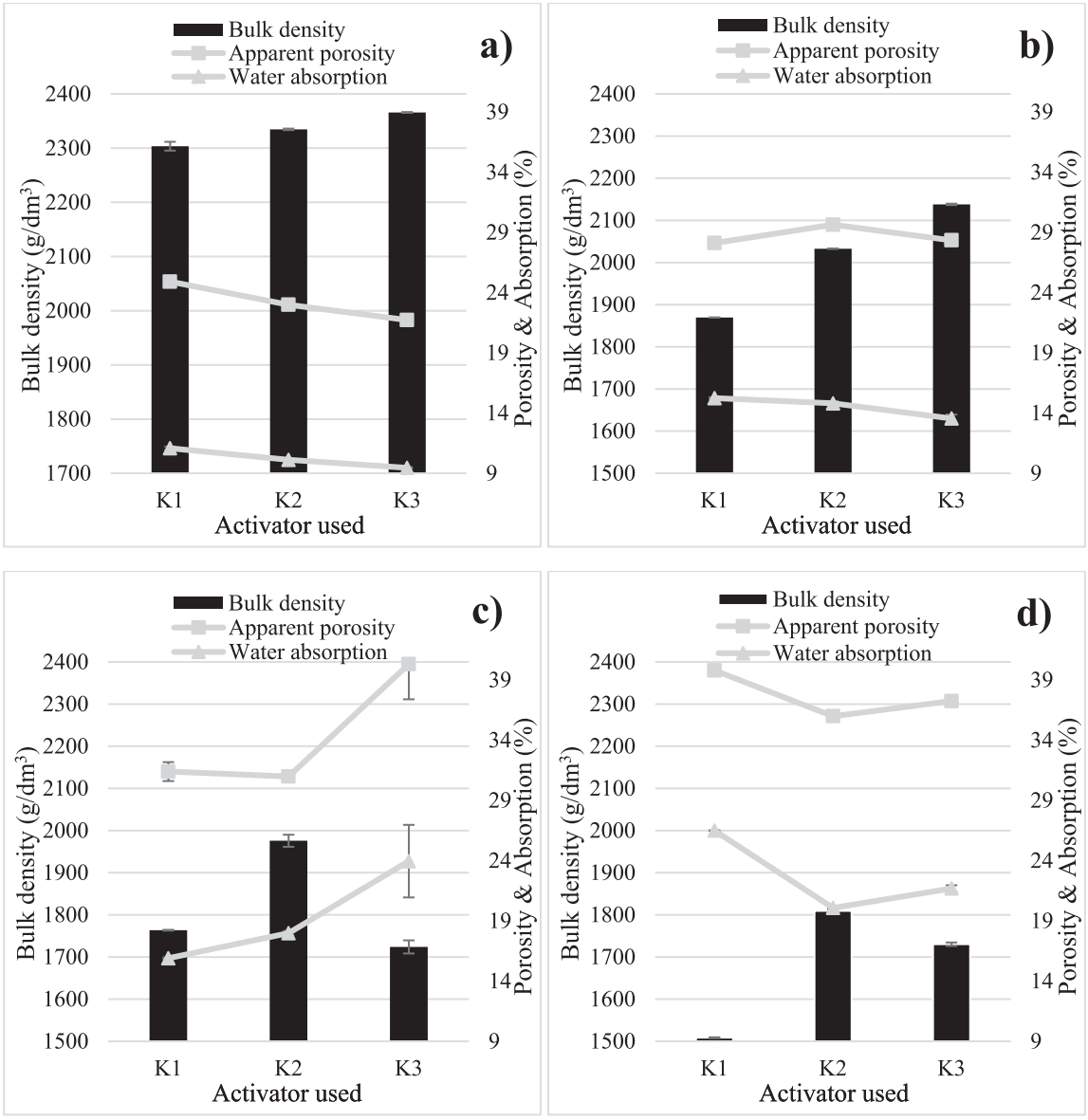

Fig. 12. Physical properties at 56 days as a function of Ms ratio: a) Control, b) 25AGA, c) 50AGA and d) 75AGA.

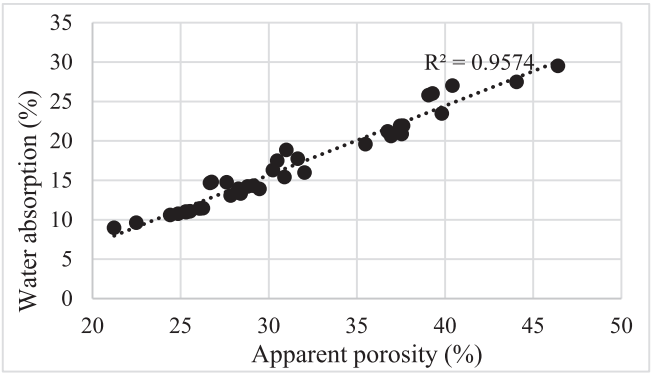

Fig. 13. Apparent porosity – Water absorption relationship.

varied from 2308 to 2335 kg/m^3, between 7 and 56 days of curing. Taking into account any activator, values fluctuated from 2279 to 2335 kg/m^3. The best specimen, in terms of mechanical strength, 25AGA samples obtained a range value between 1807 and 2138 kg/m^3. The greatest differences between samples were obtained for 50AGA, with values from 1570 to 1976 kg/m^3. Trend that was also observed for 75AGA, with bulk density between 1495 and 1730 kg/m^3. The lowest bulk densities were determined for 100AGA, between 1210 and 1418 kg/m^3. Although all samples increased bulk density values from 7 to 56 days of curing, there are some specimens in which a decrease is observed at 28 days with increasing values at 56 days of curing.

Regarding to the influence of the activator module, Ms (Fig. 12) it is observed that for the control samples or low ash samples (25 wt% AGA), the bulk density increased with increasing Ms ratio. The higher Ms ratio in the activator, the higher silica content, resulting in higher densification and lower porosity observed, as well as an increase of compressive strength [23,71]. This behaviour was not observed in samples with more ash content, where optimal activator to develop a dense matrix was K2. This is due to excess silica in the K3 activator (Ms = 1.84) which inhibits alkaline reactions, producing a less dense matrix and decreasing compressive strength [21]. However, the differences in bulk density using only slag or only ash were greater using K1 as activator. This difference decreased, increasing Ms ratio. As the case of compressive

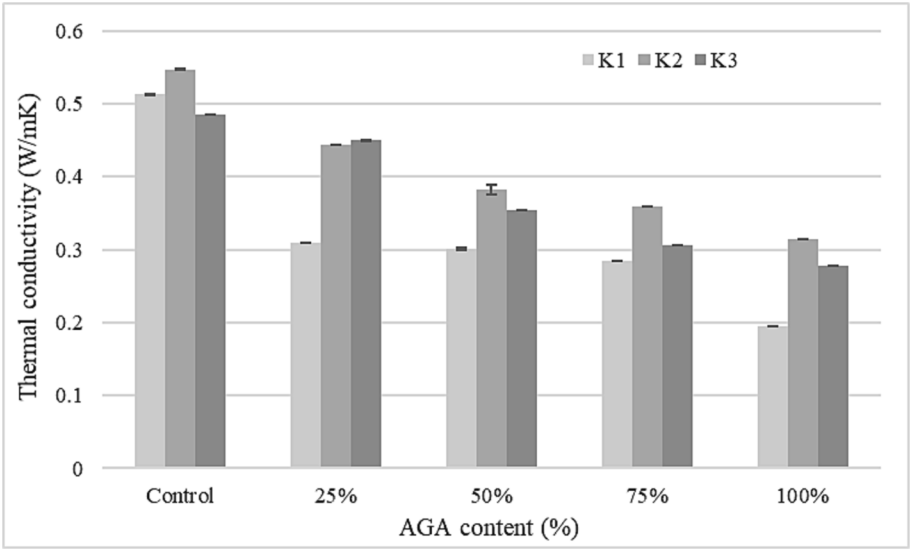

Fig. 14. Thermal conductivity of AACs at 28 days of curing.

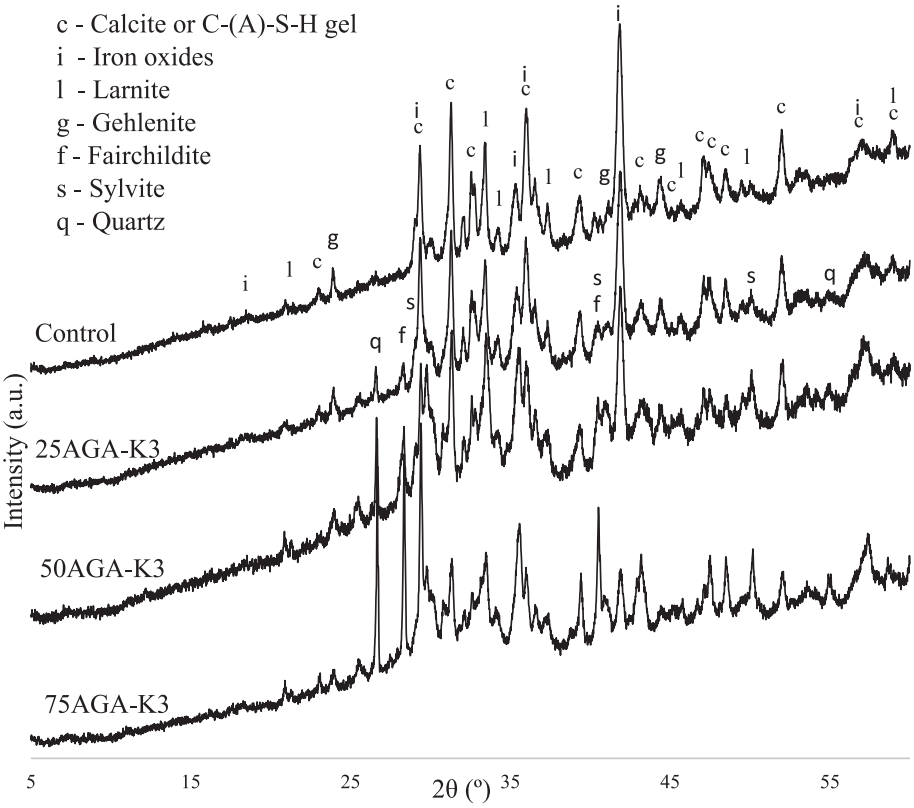

Fig. 15. DRX spectra at 28 days of curing with different ash content.

Table 4
Semi-quantitative analysis performed for samples as a function of AGA content and using K3 activator at 28 days of curing.

	Calcite-CSH gel	Iron oxides	Larnite	Gehlenite	Fairchildite	Sylvite	Quartz
Control	48	16	37	<1	<1	–	–
25AGA	48	14	33	<1	<1	2	3
50AGA	46	14	31	<1	<1	5	5
75AGA	44	9	28	<1	<1	10	8

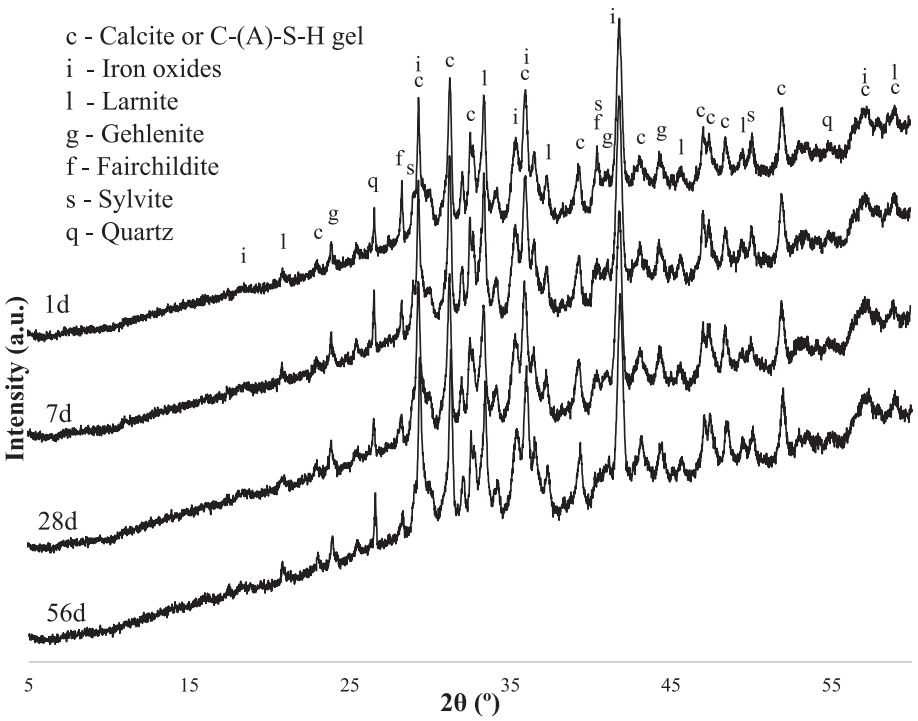

Fig. 16. DRX spectra of 25AGA as a function of curing time.

Table 5
Semi-quantitative analysis performed for 25AGA-K3 samples as a function of curing days.

	Calcite-CSH gel	Iron oxides	Larnite	Gehlenite	Fairchildite	Sylvite	Quartz
1d	42	14	34	<1	<1	2	8
7d	36	14	37	<1	<1	2	10
28d	48	14	33	<1	<1	2	3
56d	40	11	38	<1	<1	2	10

strength, an optimal value of Ms was found for the control and 25AGA samples, and a different one for the rest of the samples with higher ash content. The range of optimal values of Ms was between 1.38 and 1.84.

Water absorption affects the durability of samples, [20], so it is another important property to evaluate. Water absorption increase with increasing of amount of ash in the alkali activated materials [58], reaching its lowest value when only slags were used (8.96% at 56 days of curing of control pastes). The curing time also affect to water absorption, decreasing values when curing time is increased. The decrease in water absorption with curing time could be due to the pore structure improvement leading to an improvement in compressive strength [20]. This behaviour of physical properties was found consistent with results in mechanical strength. Water absorption and apparent porosity follow the same trend, opposite to bulk density. An increase of apparent porosity was observed when water absorption increased (Fig. 13) [95].

3.4. Thermal properties

Thermal conductivity results are shown in the Fig. 14. This property is influenced by parameters as humidity, temperature, or density [96]. Specimens with higher ash content resulted in lower thermal conductivity developed and higher thermal insulation capacity [34]. In addition, differences are also observed depending on the activator used. When the optimal activator is used, the value of thermal conductivity goes up. This behaviour is according with results obtained in physical and mechanical properties.

3.5. Structural analysis

Diffractograms of XRD obtained from pastes at 28 days of curing (Fig. 15) show calcite ($CaCO_3$), C-(A)-S-H and iron oxides as main crystalline phases. The presence of C-(A)-S-H gel and K-(A)-S-H gel were confirmed with the hump between 25°-35° [86,89,97], coexisting both in all compositions. The peak centred at 29° is associated to C-(A)-S-H gel identification [70,97]. The intensity of this peak decrease when the amount of ash increase [70]. The crystalline phase of calcite was identified (see Table 4). This pattern is overlapped with C-(A)-S-H gel, as a result of carbonation of samples during curing process [98].

In all samples, promoting the conversion of K-(A)-S-H gel into C-(A)-S-H gel. The reason is the presence of a higher quantity of Ca in both waste, which together to high pH (>12) promotes the conversion or degradation of K-(A)-S-H gel in favour of the C-(A)-S-H gel [50,99]. Other authors also observed that a higher Ca content favoured the formation of C-(A)-S-H together with K-(A)-S-H [65], or the formation of hybrid gel: K-C-(A)-S-H. The significant content of SO_3 in ashes hindered the precipitation of ettringite, which appears as traces in control pastes, affecting to the hydration and formation of C-(A)-S-H gel [100]. This is another reason of the increase of compressive strength in samples with 25 wt% ash addition.

Comparing the diffractograms of the 25CGA specimen at different curing times (Fig. 16 and Table 5), it is verified that the intensities of peaks change with time. Thus, the increase in the intensity of the peaks attributed to the C-(A)-S-H gel with curing time indicates the increased formation of this phase. The increment of the amount of gel causes an improvement in mechanical and physical properties, as it shown in

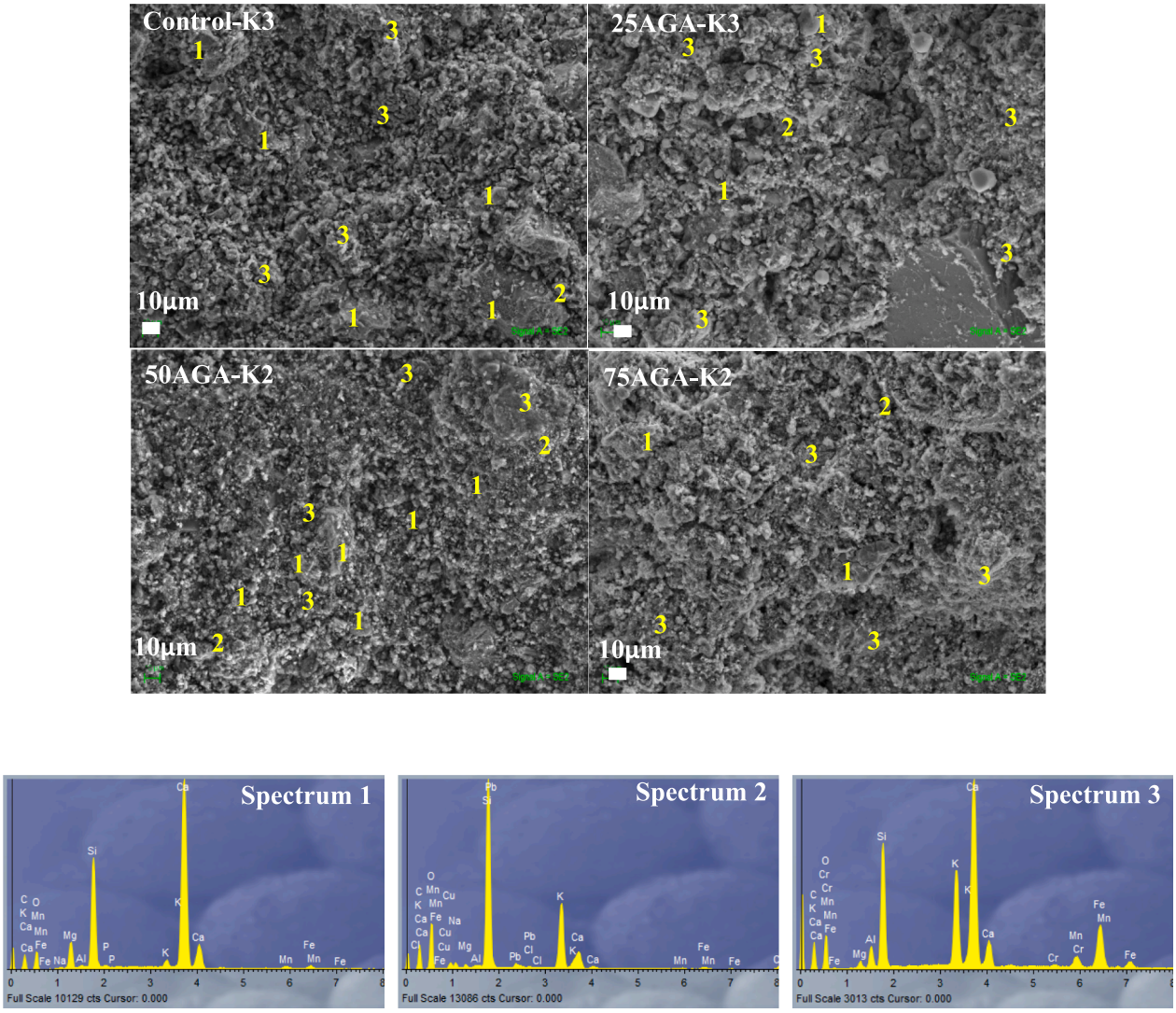

Fig. 17. SEM images of AAMs with different AGA content and alkaline activator.

previous sections.

SEM images at 28 days of curing with different content of AGA (Fig. 17) show that AACs with higher content of EAFS present a structure more dense, with less porous. Moreover, it was identified that the crystallinity increased with the increase in slags, which is attributed to greater gel formation [71]. The porosity of samples, are small porous, not resulting in any case large porous. However, when the slag content is low, the porosity is very high in accordance with apparent porosity and water absorption data, which affects to mechanical properties. This trend was observed in other studies, although with smaller amounts of replacement material [70].

EDS spectra show the coexistence of identified gels in previous sections: C-(A)-S-H gel, K-(A)-S-H gel and K-C-(A)-S-H hybrid gel. The formation of C-(A)-S-H gel is identified with the appearance of intense peaks of Si, Al and Ca (spectrum 1); while for the K-(A)-S-H gel, it is related to intense points of Si, Al and K (spectrum 2). In addition, there are areas with slightly intense peaks of Ca or K, which together with one of the previous gels, they show the possible formation of K-C-(A)-S-H hybrid gel (spectrum 3) [34,61]. In the other hand, it was observed the decrease of density with adding AGA, worsening compressive strength and showing less glassy texture, indicative of decreased gel formation [71].

Micrographs of control sample and 25AGA pastes with different Ms ratio in the activator at 28 days of curing are shown in Fig. 18. It can be seen that using an activator with low Ms, greater porosity is formed. By increasing the Ms ratio, pores are filled, reducing porosity and increasing the bulk density. For this reason, there is an increase in compressive strength when Ms is increased. Besides, the detail image of control paste using K1 and at 28 days of curing (Fig. 18-a2) confirm the appearance of ettringite as expansion product of alkali activated cement [74,75]. Comparing 25AGA-K1 and 25AGA-K3, it is also observed that using a low Ms (higher KOH content), fluorescences appear as a consequence of excess of potassium hydroxide (Fig. 18-c2 and Fig. 18-d2) [101].

4. Conclussion

An investigation using electric arc furnace slags (EAFS) as raw material, with different percentage of replacement by char from acorn gasification process (AGA) and three different activators modulus (Ms = 0.89 (K1), Ms = 1.38 (K2) and Ms = 1.84 (K3)) has been developed. The following conclusions can be drawn:

- Compressive strength exhibited a marked improvement, particularly up to the incorporation of 50 wt% AGA, exceeding control pastes (100 wt% EAFS). The composition with greater mechanical strength was 25AGA using K3 as activator, achieving a compressive strength of 30 MPa at 56 days of curing.

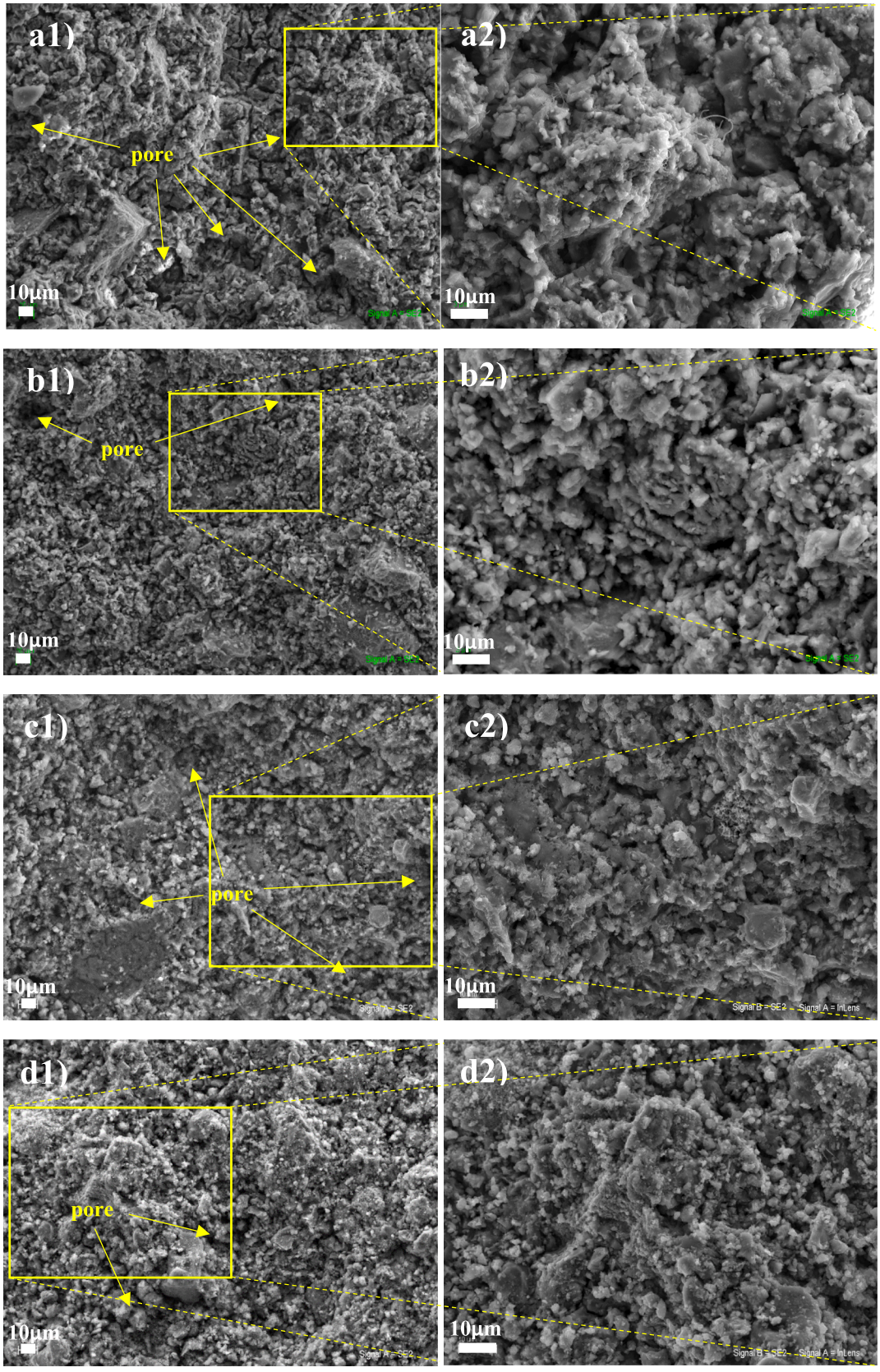

Fig. 18. SEM images of pastes with different Ms in the activator: a) Control-K1 at 1000x secondary image and 3000x back-scattered electro image; b) Control-K3 at 1000x secondary image and 3000x back-scattered electro image; c) 25AGA-K1 at 1000x and 2000x; d) 25AGA-K3 at 1000x and 2000x.

- The addition of up to 50 wt% AGA results in alkali activated cements with higher mechanical strength, due to the higher formation of C-(A)-S-H gel, K-(A)-S-H gel and C-K-(A)-S-H hybrid gel in both control samples and samples containing up to 50 wt% of AGA. Incorporation of up to 50 wt% of AGA favoured the alkali activation of EAFS slags. Increasing the AGA content above 50 wt%, weakened the matrix strength due to the paste viscosity and lower dissolution of reactive species. Thus the matrix formed was less homogeneous, and more unreacted particles and greater porosity appeared, culminating in diminished mechanical strength.
- Compressive strength data underscored that the optimal activator ratio increases with higher AGA content. Notably, lower Ms values (less than1) led to the formation of alkali activated cements characterized by reduced compressive strength. Hence, it is imperative to consider both activator ratio and AGA content simultaneously to achieve the desired compressive strength.
- The microstructural analysis revealed the presence of C-(A)-S-H, K-(A)-S-H and C-K-(A)-S-H gel in all compositions. Predominantly, C-(A)-S-H gel with a chain structure was identified as the primary reaction product in all samples. Structures highly polymerized, such as K-(A)-S-H or C-K-(A)-S-H hybrid gel, were observed to a lesser extent.

In light of the findings, it can be concluded that biomass char derived from the gasification process could be used as a precursor material in the manufacture of alkaline-activated materials, when combined with conventionally used materials like EAFS, to enhance their properties. This approach contributes to the reduction of solid waste disposal in landfills, thereby aiding in the mitigation of greenhouse gas emissions and energy consumption compared to conventional Portland cement production. Nonetheless, a thorough examination of the impact of chlorine content on steel bars in reinforced concrete structures is warranted. Such an approach would enable the generation of high-value products with considerable benefits.

CRediT authorship contribution statement

M.A. Gómez-Casero: Writing – review & editing, Writing – original draft, Methodology, Investigation, Formal analysis, Data curation, Conceptualization. **Luís Calado:** Writing – review & editing, Investigation, Formal analysis, Data curation. **Pedro Romano:** Writing – review & editing, Supervision, Resources. **D. Eliche-Quesada:** Writing – review & editing, Supervision, Funding acquisition, Conceptualization.

Declaration of Competing Interest

The authors declare that they have no known competing financial interests or personal relationships that could have appeared to influence the work reported in this paper.

Data availability

Data will be made available on request.

Acknowledgments

This work has been funded by the project PID2020-115161RB-I00: Applying the circular economy in the development of new low carbon footprint alkaline activated hydraulic binders for construction solutions (CongActiva), MCIN/AEI/10.13039/501100011033 FEDER "A way of making Europe and by the project MAT2017-88097-R: Development and characterization of new geopolymeric composites based on waste from the olive industry. Towards a sustainable construction, FEDER/Ministry of Science, Innovation and Universities, State Research Agency. Authors thank LandFood project (PV20-0050) funded by La Caixa foundation for supplying acorn, and authors also thank Siderúrgica Balboa company for supplying slags. M.A. Gómez-Casero acknowledges support of MINECO (PRE2018-084073) and the help provided by IPP and VALORIZA. Technical and human support provided by CICT of Universidad de Jaén (UJA, MINECO, Junta de Andalucía, FEDER) is gratefully acknowledged.

References

[1] P. Murugesan, V. Raja, S. Dutta, J.A. Moses, C. Anandharamakrishnan, Food waste valorisation via gasification–a review on emerging concepts, prospects and challenges, Sci. Total Environ. 157955 (2022), https://doi.org/10.1016/j.scitotenv.2022.157955.
[2] S. Valizadeh, H. Hakimian, A. Farooq, B.H. Jeon, W.H. Chen, S.H. Lee, S.C. Jung, M.W. Seo, Y.K. Park, Valorization of biomass through gasification for green hydrogen generation: a comprehensive review, Bioresour. Technol. 365 (2022), 128143, https://doi.org/10.1016/j.biortech.2022.128143.
[3] O. Alves, L. Calado, R.M. Panizio, M. Gonçalves, E. Monteiro, P. Brito, Techno-economic study for a gasification plant processing residues of sewage sludge and solid recovered fuels, Waste Manag. 131 (2021) 148–162, https://doi.org/10.1016/j.wasman.2021.05.026.
[4] R. Xiao, Q. Nie, J. He, H. Lu, Z. Shen, B. Huang, Utilizing lowly-reactive coal gasification fly ash (CGFA) to stabilize aggregate bases, J. Clean. Prod. 370 (2022), 133320, https://doi.org/10.1016/j.jclepro.2022.133320.
[5] R. Alejano, R. Tapias, M. Fernández, E. Torres, J. Alaejos, J. Domingo, Influence of pruning and the climatic conditions on acorn production in holm oak (Quercus ilex L.) dehesas in SW Spain, Ann. For. Sci. 65 (2) (2008) 1, https://doi.org/10.1051/forest:2007092.
[6] F.B. Navarro, A.B. Caño, C. Gálvez, A. Kazani, M.D. Carbonero, M.N. Jiménez, Key factors in direct acorn seeding for the successful restoration of open oak woodlands, For. Ecol. Manage. 546 (2023), 121314, https://doi.org/10.1016/j.foreco.2023.121314.
[7] R. Puig-Gironès, M. Muriana, J. Real, S. Sabaté, Unravelling the influence of annual weather conditions and Mediterranean habitat types on acorn production, availability and predation, For. Ecol. Manage. 543 (2023), 121149, https://doi.org/10.1016/j.foreco.2023.121149.
[8] L. Pérez-Camacho, P. Villar-Salvador, J.A. Cuevas, T. González-Sousa, L. Martínez-Baroja, Spatial decision-making in acorn dispersal by Eurasian jays around the forest edge: Insights into oak forest regeneration mechanisms, For. Ecol. Manage. 545 (2023), 121291, https://doi.org/10.1016/j.foreco.2023.121291.
[9] S. Garcia-Barreda, C. Valeriano, J.J. Camarero, Drought constrains acorn production and tree growth in the Mediterranean holm oak and triggers weak legacy effects, Agric. For. Meteorol. 334 (2023), 109435, https://doi.org/10.1016/j.agrformet.2023.109435.
[10] I. Gkountenoudi-Eskitzi, K. Kotsiou, M.N. Irakli, A. Lazaridis, C.G. Biliaderis, A. Lazaridou, In vitro and in vivo glycemic responses and antioxidant potency of acorn and chickpea fortified gluten-free breads, Food Res. Int. 166 (2023), 112579, https://doi.org/10.1016/j.foodres.2023.112579.
[11] J. Xu, C. Fu, T. Li, X. Xia, H. Zhang, X. Wang, Y. Zhao, Protective effect of acorn (Quercus liaotungensis Koidz) on streptozotocin-damaged MIN6 cells and type 2 diabetic rats via p38 MAPK/Nrf2/HO-1 pathway, J. Ethnopharmacol. 266 (2021), 113444, https://doi.org/10.1016/j.jep.2020.113444.
[12] C. Reyes-Palomo, E. Aguilera, M. Llorente, C. Díaz-Gaona, G. Moreno, V. Rodríguez-Estévez, Free-range acorn feeding results in negative carbon footprint of Iberian pig production in the dehesa agro-forestry system, J. Clean. Prod. 418 (2023), 138170, https://doi.org/10.1016/j.jclepro.2023.138170.
[13] J. Rojo, A. George, L. Ramjan, L. Hunt, Y. Salamonson, Development and psychometric testing of the attitude and confidence with oral healthcare among nursing students (ACORN) scale, Nurse Educ. Pract. 71 (2023), 103736, https://doi.org/10.1016/j.nepr.2023.103736.
[14] F. Mezni, B. Stiti, S. Fkiri, F. Ayari, L.B. Slimane, R. Ksouri, A. Khaldi, Phenolic profile and in vitro anti-diabetic activity of acorn from four African Quercus species (Q. suber, Q. canariensis, Q. coccifera and Q. ilex), S. Afr. J. Bot. 146 (2022) 771–775, https://doi.org/10.1016/j.sajb.2021.12.023.
[15] S. Ferreira, E. Monteiro, L. Calado, V. Silva, P. Brito, C. Vilarinho, Experimental and modeling analysis of brewerś spent grains gasification in a downdraft reactor, Energies 12 (23) (2019) 4413, https://doi.org/10.3390/en12234413.
[16] J. Qu, J. Zhang, H. Li, S. Li, A high value utilization process for coal gasification slag: Preparation of high modulus sodium silicate by mechano-chemical synergistic activation, Sci. Total Environ. 801 (2021), 149761, https://doi.org/10.1016/j.scitotenv.2021.149761.
[17] Q. Qiao, H. Zhou, F. Guo, R. Shu, S. Liu, L. Xu, K. Dongf, Y. Bai, Facile and scalable synthesis of mesoporous composite materials from coal gasification fine slag for enhanced adsorption of malachite green, J. Clean. Prod. 134739 (2022), https://doi.org/10.1016/j.jclepro.2022.134739.
[18] P. Duxson, J.L. Provis, G.C. Lukey, S.W. Mallicoat, W.M. Kriven, J.S. Van Deventer, Understanding the relationship between geopolymer composition, microstructure and mechanical properties, Colloids Surf. A 269 (1–3) (2005) 47–58, https://doi.org/10.1016/j.colsurfa.2005.06.060.
[19] H.S. Gökçe, M. Tuyan, M.L. Nehdi, Alkali-activated and geopolymer materials developed using innovative manufacturing techniques: A critical review, Constr. Build. Mater. 303 (2021), 124483, https://doi.org/10.1016/j.conbuildmat.2021.124483.

[20] A.M. Rashad, S.A. Khafaga, M. Gharieb, Valorization of fly ash as an additive for electric arc furnace slag geopolymer cement, Constr. Build. Mater. 294 (2021), 123570, https://doi.org/10.1016/j.conbuildmat.2021.123570.
[21] M. Ozturk, M.B. Bankir, O.S. Bolukbasi, U.K. Sevim, Alkali activation of electric arc furnace slag: Mechanical properties and micro analyzes, J Build Eng 21 (2019) 97–105, https://doi.org/10.1016/j.jobe.2018.10.005.
[22] T. Xie, P. Visintin, A unified approach for mix design of concrete containing supplementary cementitious materials based on reactivity moduli, J. Clean. Prod. 203 (2018) 68–82, https://doi.org/10.1016/j.jclepro.2018.08.254.
[23] M. Nawaz, A. Heitor, M. Sivakumar, Geopolymers in construction-recent developments, Constr. Build. Mater. 260 (2020), 120472, https://doi.org/10.1016/j.conbuildmat.2020.120472.
[24] I. Nikolić, A. Drinčić, D. Djurović, L. Karanović, V.V. Radmilović, V. R. Radmilović, Kinetics of electric arc furnace slag leaching in alkaline solutions, Constr. Build. Mater. 108 (2016) 1–9, https://doi.org/10.1016/j.conbuildmat.2016.01.038.
[25] A. Aziz, A. Bellil, I.E.E.A. El Hassani, M. Fekhaoui, M. Achab, A. Dahrouch, A. Benzaouak, Geopolymers based on natural perlite and kaolinic clay from Morocco: Synthesis, characterization, properties, and applications, Ceram. Int. 47 (17) (2021) 24683–24692, https://doi.org/10.1016/j.ceramint.2021.05.190.
[26] A.B. Shinkafi, M. Khorami, E. Ganjian, M. Tyrer, Influence of alkali activator type and proportion on strength performance of calcined clay geopolymer mortar, Constr. Build. Mater. 267 (2021), 120446, https://doi.org/10.1016/j.conbuildmat.2020.120446.
[27] M.A. Gómez-Casero, F.J. Moral-Moral, L. Pérez-Villarejo, P.J. Sánchez-Soto, D. Eliche-Quesada, Synthesis of clay geopolymers using olive pomace fly ash as an alternative activator. Influence of the additional commercial alkaline activator used, J. Mater. Res. Technol. 12 (2021) 1762–1776, https://doi.org/10.1016/j.jmrt.2021.03.102.
[28] Y. Luo, J. Meng, D. Wang, L. Jiao, G. Xue, Experimental study on mechanical properties and microstructure of metakaolin based geopolymer stabilized silty clay, Constr. Build. Mater. 316 (2022), 125662, https://doi.org/10.1016/j.conbuildmat.2021.125662.
[29] A. Gharzouni, B. Samet, S. Baklouti, E. Joussein, S. Rossignol, Addition of low reactive clay into metakaolin-based geopolymer formulation: Synthesis, existence domains and properties, Powder Technol. 288 (2016) 212–220, https://doi.org/10.1016/j.powtec.2015.11.012.
[30] M.A. Gómez-Casero, C. De Dios-Arana, J.S. Bueno-Rodríguez, L. Pérez-Villarejo, D. Eliche-Quesada, Physical, mechanical and thermal properties of metakaolin-fly ash geopolymers, Sustain. Chem. Pharm. 26 (2022), 100620, https://doi.org/10.1016/j.scp.2022.100620.
[31] M. Kaya, F. Koksal, O. Gencel, M.J. Munir, S.M.S. Kazmi, Influence of micro Fe2O3 and MgO on the physical and mechanical properties of the zeolite and kaolin based geopolymer mortar, J. Build. Eng. 52 (2022), 104443, https://doi.org/10.1016/j.jobe.2022.104443.
[32] S. Wang, L. Yu, L. Huang, K. Wu, Z. Yang, Incorporating steel slag in the production of high heat resistant FA based geopolymer paste via pressure molding, J. Clean. Prod. 325 (2021), 129265, https://doi.org/10.1016/j.jclepro.2021.129265.
[33] M.T. Marvila, A.R.G. de Azevedo, J.A.T.L. Júnior, C.M.F. Vieira, Activated alkali cement based on blast furnace slag: effect of curing type and concentration of Na20, J. Mater. Res. Technol. 23 (2023) 4551–4565, https://doi.org/10.1016/j.jmrt.2023.02.088.
[34] M.A. Gómez-Casero, L. Pérez-Villarejo, E. Castro, D. Eliche-Quesada, Effect of steel slag and curing temperature on the improvement in technological properties of biomass bottom ash based alkali-activated materials, Constr. Build. Mater. 302 (2021), 124205, https://doi.org/10.1016/j.conbuildmat.2021.124205.
[35] C. Bai, Y. Deng, Q. Zhou, G. Deng, T. Yang, Y. Yang, Effect of different curing methods on the preparation of carbonized high-titanium slag based geopolymers, Constr. Build. Mater. 342 (2022), 128023, https://doi.org/10.1016/j.conbuildmat.2022.128023.
[36] M.A. Gómez-Casero, L. Pérez-Villarejo, P.J. Sánchez-Soto, D. Eliche-Quesada, Comparative study of alkali activated cements based on metallurgical slags, in terms of technological properties developed, Sustain. Chem. Pharm. 29 (2022), 100746, https://doi.org/10.1016/j.scp.2022.100746.
[37] J. Tang, P. Liu, S. Xue, Y. Li, Y. Zhao, K. Huang, Z. Liu, Optimization of coal fly ash-based porous geopolymer synthesis and application for zinc removal from water, Ceram. Int. 49 (4) (2022) 5828–5833, https://doi.org/10.1016/j.ceramint.2022.10.028.
[38] C. Fan, B. Wang, H. Ai, Y. Qi, Z. Liu, A comparative study on solidification/stabilization characteristics of coal fly ash-based geopolymer and Portland cement on heavy metals in MSWI fly ash, J. Clean. Prod. 319 (2021), 128790, https://doi.org/10.1016/j.jclepro.2021.128790.
[39] Z. Liu, P. Deng, Z. Zhang, Application of silica-rich biomass ash solid waste in geopolymer preparation: a review, Constr. Build. Mater. 356 (2022), 129142, https://doi.org/10.1016/j.conbuildmat.2022.129142.
[40] A. De Rossi, L. Simão, M.J. Ribeiro, D. Hotza, R.F.P.M. Moreira, Study of cure conditions effect on the properties of wood biomass fly ash geopolymers, J. Mater. Res. Technol. 9 (4) (2020) 7518–7528, https://doi.org/10.1016/j.jmrt.2020.05.047.
[41] R.M. Novais, G. Ascensao, D.M. Tobaldi, M.P. Seabra, J.A. Labrincha, Biomass fly ash geopolymer monoliths for effective methylene blue removal from wastewaters, J. Clean. Prod. 171 (2018) 783–794, https://doi.org/10.1016/j.jclepro.2017.10.078.
[42] P. Arokiasamy, M.M.A.B. Abdullah, S.Z. Abd Rahim, M.R.R.M.A. Zainol, M.A.A. M. Salleh, M. Kheimi, J. Chaiprapa, A.V. Sandu, P. Vizureanu, R.A. Razak, N. H. Jamil, Metakaolin/sludge based geopolymer adsorbent on high removal efficiency of Cu2+, Case Stud. Constr. Mater. 17 (2022) e01428.
[43] N.B. da Silva Nuernberg, D.F. Niero, A.M. Bernardin, Valorization of rice husk ash and aluminum anodizing sludge as precursors for the synthesis of geopolymers, J. Clean. Prod. 298 (2021), 126770, https://doi.org/10.1016/j.jclepro.2021.126770.
[44] Y. Gao, T. Guo, Z. Li, Z. Zhou, J. Zhang, Mechanism of retarder on hydration process and mechanical properties of red mud-based geopolymer cementitious materials, Constr. Build. Mater. 356 (2022), 129306, https://doi.org/10.1016/j.conbuildmat.2022.129306.
[45] S.M.A. Qaidi, B.A. Tayeh, H.U. Ahmed, W. Emad, A review of the sustainable utilisation of red mud and fly ash for the production of geopolymer composites, Constr. Build. Mater. 350 (2022), 128892, https://doi.org/10.1016/j.conbuildmat.2022.128892.
[46] Z. Sun, Q. Tang, B.S. Xakalashe, X. Fan, M. Gan, X. Chen, Z. Ji, X. Huang, B. Friedrich, Mechanical and environmental characteristics of red mud geopolymers, Constr. Build. Mater. 321 (2022), 125564, https://doi.org/10.1016/j.conbuildmat.2021.125564.
[47] G.A. Tochetto, L. Simão, D. de Oliveira, D. Hotza, A.P.S. Immich, Porous geopolymers as dye adsorbents: Review and perspectives, J. Clean. Prod. 133982 (2022), https://doi.org/10.1016/j.jclepro.2022.133982.
[48] M.A. Villaquirán-Caicedo, R.M. de Gutiérrez, Comparison of different activators for alkaline activation of construction and demolition wastes, Constr. Build. Mater. 281 (2021), 122599, https://doi.org/10.1016/j.conbuildmat.2021.122599.
[49] T. Lan, Y. Meng, T. Ju, Z. Chen, Y. Du, Y. Deng, M. Song, S. Han, J. Jiang, Synthesis and application of geopolymers from municipal waste incineration fly ash (MSWI FA) as raw ingredient-A review, Resour. Conserv. Recycl. 182 (2022), 106308, https://doi.org/10.1016/j.resconrec.2022.106308.
[50] M. Alhawat, A. Ashour, G. Yildirim, A. Aldemir, M. Sahmaran, Properties of geopolymers sourced from construction and demolition waste: A review, J Build Eng 50 (2022), 104104, https://doi.org/10.1016/j.jobe.2022.104104.
[51] X. He, Z. Yuhua, S. Qaidi, H.F. Isleem, O. Zaid, F. Althoey, J. Ahmad, Mine tailings-based geopolymers: A comprehensive review, Ceram. Int. 48 (17) (2022) 24192–24212, https://doi.org/10.1016/j.ceramint.2022.05.345.
[52] N. Elmesalami, K. Celik, A critical review of engineered geopolymer composite: A low-carbon ultra-high-performance concrete, Constr. Build. Mater. 346 (2022), 128491, https://doi.org/10.1016/j.conbuildmat.2022.128491.
[53] P. Yang, L. Liu, Y. Suo, G. Xie, W. Sun, C. Zhang, Physical-chemical coupling excitation of low activity coal gasification slag solid waste and its application as a backfill cementitious material, Constr. Build. Mater. 401 (2023), 132973, https://doi.org/10.1016/j.conbuildmat.2023.132973.
[54] Y. Li, C. Wei, X. Liu, Z. Zhang, J. Wan, X. He, Application of gasification slag in construction materials and high value-added materials: a review, Constr. Build. Mater. 402 (2023), 133013, https://doi.org/10.1016/j.conbuildmat.2023.133013.
[55] Y. Chen, X. Zhou, S. Wan, R. Zheng, J. Tong, H. Hou, T. Wang, Synthesis and characterization of geopolymer composites based on gasification coal fly ash and steel slag, Constr. Build. Mater. 211 (2019) 646–658, https://doi.org/10.1016/j.conbuildmat.2019.03.292.
[56] X. Zhou, Y. Chen, S. Dong, H. Li, Geopolymerization kinetics of steel slag activated gasification coal fly ash: A case study for amorphous-rich slags, J. Clean. Prod. 134671 (2022), https://doi.org/10.1016/j.jclepro.2022.134671.
[57] Y. Chen, F. Chen, F. Zhou, M. Lu, H. Hou, J. Li, D. Liu, T. Wang, Early solidification/stabilization mechanism of heavy metals (Pb, Cr and Zn) in Shell coal gasification fly ash based geopolymer, Sci. Total Environ. 802 (2022), 149905, https://doi.org/10.1016/j.scitotenv.2021.149905.
[58] E. Furlani, S. Maschio, M. Magnan, E. Aneggi, F. Andreatta, M. Lekka, A. Lanzutti, L. Fedrizzi, Synthesis and characterization of geopolymers containing blends of unprocessed steel slag and metakaolin: The role of slag particle size, Ceram. Int. 44 (5) (2018) 5226–5232, https://doi.org/10.1016/j.ceramint.2017.12.131.
[59] Y. Zhang, E. Schlangen, O. Çopuroğlu, Effect of slags of different origins and the role of sulfur in slag on the hydration characteristics of cement-slag systems, Constr. Build. Mater. 316 (2022), 125266, https://doi.org/10.1016/j.conbuildmat.2021.125266.
[60] G. Kaladharan, F. Rajabipour, Evaluation and beneficiation of high sulfur and high alkali fly ashes for use as supplementary cementitious materials in concrete, Constr. Build. Mater. 339 (2022), 127672, https://doi.org/10.1016/j.conbuildmat.2022.127672.
[61] L. Soriano, A. Font, M.V. Borrachero, J.M. Monzó, J. Payá, M.M. Tashima, Biomass ashes to produce an alternative alkaline activator for alkali-activated cements, Mater. Lett. 308 (2022), 131198, https://doi.org/10.1016/j.matlet.2021.131198.
[62] F.S. Lima, T.C.F. Gomes, J.C.B. Moraes, Effect of coffee husk ash as alkaline activator in one-part alkali-activated binder, Constr. Build. Mater. 362 (2023), 129799, https://doi.org/10.1016/j.conbuildmat.2022.129799.
[63] F.A. Ferreira, J.M. Desir, G.E.S. De Lima, L.G. Pedroti, J.M.F. De Carvalho, A. Lotero, N.C. Consoli, Evaluation of mechanical and microstructural properties of eggshell lime/rice husk ash alkali-activated cement, Constr. Build. Mater. 364 (2023), 129931, https://doi.org/10.1016/j.conbuildmat.2022.129931.
[64] I. Ismail, S.A. Bernal, J.L. Provis, R. San Nicolas, S. Hamdan, J.S. van Deventer, Modification of phase evolution in alkali-activated blast furnace slag by the incorporation of fly ash, Cem. Concr. Compos. 45 (2014) 125–135, https://doi.org/10.1016/j.cemconcomp.2013.09.006.
[65] N. Hui-Teng, H. Cheng-Yong, L. Yun-Ming, M.M.A.B. Abdullah, K.E. Hun, H. M. Razi, N. Yong-Sing, Formulation, mechanical properties and phase analysis of

fly ash geopolymer with ladle furnace slag replacement, J. Mater. Res. Technol. 12 (2021) 1212–1226, https://doi.org/10.1016/j.jmrt.2021.03.065.
[66] N.Y. Mostafa, S.A.S. El-Hemaly, E.I. Al-Wakeel, S.A. El-Korashy, P.W. Brown, Characterization and evaluation of the hydraulic activity of water-cooled slag and air-cooled slag, Cem. Concr. Res. 31 (6) (2001) 899–904, https://doi.org/10.1016/S0008-8846(01)00497-5.
[67] UNE-EN 1015-11: 2000/A1: 2007. (1999). Methods of Test for Mortar for Masonry—Part 11: Determination of Flexural and Compressive Strength of Hardened Mortar.
[68] UNE-EN 1015-10: 2000. (2000). Methods of Test for Mortar for Masonry—Part 10: Determination of Dry Bulk Density of Hardened Mortar.
[69] Asociación Española de Normalización y Certificación (AENOR). Thermal Performance of Building Materials and Products—Determination of Thermal Resistance by Means of Guarded Hot Plate and Heat Flow Meter Methods: Dry and Moist Products of Medium and Low Thermal Resistance; UNE-EN 12664: 2002; AENOR: Madrid, Spain, 2002.
[70] J. He, R. Xiao, Q. Nie, J. Zhong, B. Huang, High-volume coal gasification fly ash–cement systems: Experimental and thermodynamic investigation, Constr. Build. Mater. 377 (2023), 131082, https://doi.org/10.1016/j.conbuildmat.2023.131082.
[71] A. Rafeet, R. Vinai, M. Soutsos, W. Sha, Effects of slag substitution on physical and mechanical properties of fly ash-based alkali activated binders (AABs), Cem. Concr. Res. 122 (2019) 118–135, https://doi.org/10.1016/j.cemconres.2019.05.003.
[72] V. Ponomar, E. Adesanya, K. Ohenoja, M. Illikainen, High-temperature performance of slag-based Fe-rich alkali-activated materials, Cem. Concr. Res. 161 (2022), 106960, https://doi.org/10.1016/j.cemconres.2022.106960.
[73] D.B. Istuque, L. Soriano, J.L. Akasaki, J.L.P. Melges, M.V. Borrachero, J. Monzó, M.M. Tashima, Effect of sewage sludge ash on mechanical and microstructural properties of geopolymers based on metakaolin, Constr. Build. Mater. 203 (2019) 95–103, https://doi.org/10.1016/j.conbuildmat.2019.01.093.
[74] N.A.M. Beltrame, C.A. da Luz, M. Perardt, R.D. Hooton, Alkali activated cement made from blast furnace slag generated by charcoal: Resistance to attack by sodium and magnesium sulfates, Constr. Build. Mater. 238 (2020), 117710, https://doi.org/10.1016/j.conbuildmat.2019.117710.
[75] Y. Ma, J. Qian, Influence of alkali sulfates in clinker on the hydration and hardening of Portland cement, Constr. Build. Mater. 180 (2018) 351–363, https://doi.org/10.1016/j.conbuildmat.2018.05.196.
[76] M. Shakouri, C.L. Exstrom, S. Ramanathan, P. Suraneni, J.S. Vaux, Pretreatment of corn stover ash to improve its effectiveness as a supplementary cementitious material in concrete, Cem. Concr. Compos. 112 (2020), 103658, https://doi.org/10.1016/j.cemconcomp.2020.103658.
[77] C.W. Hsu, C.T. Chen, Strength development of cement pastes with alkali-activated dehydrated sewage sludge, Constr. Build. Mater. 255 (2020), 119243, https://doi.org/10.1016/j.conbuildmat.2020.119243.
[78] A. Hussan, D. Levacher, S. Mezazigh, L. Jardin, Co-valorization of sediments incorporating high and low organic matter with alkali-activated GGBS and hydraulic binder for use in road construction, J Build Eng 105848 (2023), https://doi.org/10.1016/j.jobe.2023.105848.
[79] J. Liu, Z. Wang, G. Xie, Z. Li, X. Fan, W. Zhang, J. Ren, Resource utilization of municipal solid waste incineration fly ash-cement and alkali-activated cementitious materials: A review, Sci. Total Environ. 158254 (2022), https://doi.org/10.1016/j.scitotenv.2022.158254.
[80] J.W. Phair, J.S.J. Deventer, J.D. Smith, Mechanism of polysialation in the incorporation of zirconia into fly ash-based geopolymers, Ind. Eng. Chem. Res. 2000 (39) (2000) 2925–2934, https://doi.org/10.1021/ie990929w.
[81] M. Soutsos, A.P. Boyle, R. Vinai, A. Hadjierakleous, S.J. Barnett, Factors influencing the compressive strength of fly ash based geopolymers, Constr. Build. Mater. 110 (2016) 355–368, https://doi.org/10.1016/j.conbuildmat.2015.11.045.
[82] P. Zhang, L. Kang, Y. Zheng, T. Zhang, B. Zhang, Influence of SiO2/Na2O molar ratio on mechanical properties and durability of metakaolin-fly ash blend alkali-activated sustainable mortar incorporating manufactured sand, J. Mater. Res. Technol. 18 (2022) 3553–3563, https://doi.org/10.1016/j.jmrt.2022.04.041.
[83] M.M. Tashima, J.L. Akasaki, J.L.P. Melges, L. Soriano, J. Monzó, J. Payá, M. V. Borrachero, Alkali activated materials based on fluid catalytic cracking catalyst residue (FCC): Influence of SiO2/Na2O and H2O/FCC ratio on mechanical strength and microstructure, Fuel 108 (2013) 833–839, https://doi.org/10.1016/j.fuel.2013.02.052.
[84] I. Perná, M. Šupová, T. Hanzlíček, A. Špaldoňová, The synthesis and characterization of geopolymers based on metakaolin and high LOI straw ash, Constr. Build. Mater. 228 (2019), 116765, https://doi.org/10.1016/j.conbuildmat.2019.116765.
[85] G. Kovalchuk, A. Fernández-Jiménez, A. Palomo, Alkali-activated fly ash: effect of thermal curing conditions on mechanical and microstructural development–Part II, Fuel 86 (3) (2007) 315–322, https://doi.org/10.1016/j.fuel.2006.07.010.
[86] J. Li, Z. Ma, J. Gao, Y. Guo, F. Cheng, Synthesis and characterization of geopolymer prepared from circulating fluidized bed-derived fly ash, Ceram. Int. 48 (8) (2022) 11820–11829, https://doi.org/10.1016/j.ceramint.2022.01.052.
[87] M.R. Ahmad, L.P. Qian, Y. Fang, A. Wang, J.G. Dai, A multiscale study on gel composition of hybrid alkali-activated materials partially utilizing air pollution control residue as an activator, Cem. Concr. Compos. 104856 (2022), https://doi.org/10.1016/j.cemconcomp.2022.104856.
[88] D. Huang, Q. Yuan, P. Chen, X. Tian, H. Peng, Effect of activator properties on drying shrinkage of alkali-activated fly ash and slag, J Build Eng 105341 (2022), https://doi.org/10.1016/j.jobe.2022.105341.
[89] M. Criado, W. Aperador, I. Sobrados, Microstructural and mechanical properties of alkali activated Colombian raw materials, Materials 9 (3) (2016) 158, https://doi.org/10.3390/ma9030158.
[90] W.K.W. Lee, J.S.J. Deventer, Effects of anions on the formation of aluminosilicate gel in geopolymers, Ind. Eng. Chem. Res. 41 (2002) 4550–4558, https://doi.org/10.1021/ie0109410.
[91] I. Lancellotti, M. Catauro, C. Ponzoni, F. Bollino, C. Leonelli, Inorganic polymers from alkali activation of metakaolin: effect of setting and curing on structure, J. Solid State Chem. 2013 (200) (2013) 341–348, https://doi.org/10.1016/j.jssc.2013.02.003.
[92] D.W. Zhang, K.F. Zhao, D.M. Wang, H. Li, Relationship of amorphous gel-microstructure-elastoviscosity properties of alkali-activated materials fresh pastes with different Ms waterglass, Constr. Build. Mater. 287 (2021), 123023, https://doi.org/10.1016/j.conbuildmat.2021.123023.
[93] M. Criado, A. Fernández-Jiménez, A. Palomo, Alkali activation of fly ash: Effect of the SiO2/Na2O ratio: Part I: FTIR study, Microporous Mesoporous Mate 106 (1–3) (2007) 180–191, https://doi.org/10.1016/j.micromeso.2007.02.055.
[94] J. Zhang, C. Shi, Z. Zhang, Carbonation induced phase evolution in alkali-activated slag/fly ash cements: The effect of silicate modulus of activators, Constr. Build. Mater. 223 (2019) 566–582, https://doi.org/10.1016/j.conbuildmat.2019.07.024.
[95] E. Adesanya, K. Ohenoja, P. Kinnunen, M. Illikainen, Alkali activation of ladle slag from steel-making process, J Sustainable Metall 3 (2) (2017) 300–310, https://doi.org/10.1007/s40831-016-0089-x.
[96] B.S. Thomas, J. Yang, A. Bahurudeen, J.A. Abdalla, R.A. Hawileh, H.M. Hamada, S. Nazar, V. Jittin, D.K. Ashish, Sugarcane bagasse ash as supplementary cementitious material in concrete–A review, Mater Today Sustainability 15 (2021), 100086, https://doi.org/10.1016/j.mtsust.2021.100086.
[97] S.Y. Oderji, B. Chen, M.R. Ahmad, S.F.A. Shah, Fresh and hardened properties of one-part fly ash-based geopolymer binders cured at room temperature: effect of slag and alkali activators, J. Clean. Prod. 225 (2019) 1–10, https://doi.org/10.1016/j.jclepro.2019.03.290.
[98] E. Adesanya, K. Ohenoja, A. Di Maria, P. Kinnunen, M. Illikainen, Alternative alkali-activator from steel-making waste for one-part alkali-activated slag, J. Clean. Prod. 274 (2020), 123020, https://doi.org/10.1016/j.jclepro.2020.123020.
[99] B. Ren, Y. Zhao, H. Bai, S. Kang, T. Zhang, S. Song, Eco-friendly geopolymer prepared from solid wastes: A critical review, Chemosphere 267 (2021), 128900, https://doi.org/10.1016/j.chemosphere.2020.128900.
[100] M. Zajac, M. Wieczorek, B. Lothenbach, F. Bullerjahn, V.M. Schmidt, M.B. Haha, Effect of alkali and sulfate on early hydration of Portland cements at high water to cement ratio, Constr. Build. Mater. 345 (2022), 128283, https://doi.org/10.1016/j.conbuildmat.2022.128283.
[101] M.A. Longhi, E.D. Rodriguez, B. Walkley, Z. Zhang, A.P. Kirchheim, Metakaolin-based geopolymers: relation between formulation, physicochemical properties and efflorescence formation, Compos. B Eng. 182 (2020), 107671, https://doi.org/10.1016/j.compositesb.2019.107671.